5-2014

Crowdsourcing Water Quality Data Using the iPhone Camera

Thomas Leeuw

CROWDSOURCING WATER QUALITY DATA USING THE IPHONE CAMERA

By

Thomas Leeuw

B.S. University of Maine, 2012

A THESIS

Submitted in Partial Fulfillment of the

Requirements for the Degree of

Master of Science

(in Oceanography)

The Graduate School

The University of Maine

May 2014

Advisory Committee:

Emmanuel Boss, Professor of Oceanography, Advisor

Mary Jane Perry, Professor of Oceanography

Lee Karp-Boss, Professor of Oceanography

THESIS ACCEPTANCE STATEMENT

On behalf of the Graduate Committee for Thomas Leeuw, I affirm that this manuscript is the final and accepted thesis. Signatures of all committee members are on file with the Graduate School at the University of Maine, 42 Stodder Hall, Orono, Maine.

Emmanuel Boss, Professor of Oceanography (Date)

LIBRARY RIGHTS STATEMENT

In presenting this thesis in partial fulfillment of the requirements for an advanced degree at The University of Maine, I agree that the Library shall make it freely available for inspection. I further agree that permission for "fair use" copying of this thesis for scholarly purposes may be granted by the Librarian. It is understood that any copying or publication of this thesis for financial gain shall not be allowed without my written permission.

Signature: _____

Date: _____

CROWDSOURCING WATER QUALITY DATA USING THE IPHONE CAMERA

By Thomas Leeuw

Thesis Advisor: Dr. Emmanuel Boss

An Abstract of the Thesis Presented
in Partial Fulfillment of the Requirements for the
Degree of Master of Science
(in Oceanography)
May 2014

The ubiquity and advanced computing power of smartphones make them a potential tool for environmental monitoring on a global scale. In an attempt to tap this resource, a water quality application (HyrdroColor) was developed. HydroColor uses the iPhone's digital color camera as a primitive three-band radiometer. Using three images taken by the user, HydroColor calculates the remote sensing reflectance in the red, green, and blue color channels of the camera. The absolute or relative reflectance between channels can be used to obtain estimates of chlorophyll, turbidity, suspended particle material, and the backscattering coefficient. In the future, HydroColor will be linked to an online database where users can upload their measurements, thus crowdsourcing water quality data.

ACKNOWLEDGEMENTS

Thank you to Dr. Ivona Cetinic for providing radiometric data. Thank you to Katelyn Hunt and William Kardas for helping with data collection along the coast of Georgia. I would also like to thank my advisory committee for all the guidance they have provided me during my time at the University of Maine.

TABLE OF CONTENTS

LIST OF TABLES

LIST OF FIGURES

LIST OF SYMBOLS

$\mathbf{a_w}$	Absorption Coefficient of Pure Water (m^{-1})
$\mathbf{a_p}$	Particulate Absorption Coefficient (m^{-1})
$\mathbf{a_p}^*$	Mass Specific Particulate Absorption Coefficient (m^2 g^{-1})
$\mathbf{b_{bp}}$	Particulate Backscattering Coefficient (m^{-1})
$\mathbf{b_{bp}}^*$	Mass Specific Particulate Backscattering Coefficient (m^2 g^{-1})
$\mathbf{b_b}$	Backscatter Coefficient (m^{-1})
$\mathbf{B_v}$	Brightness Value
$\mathbf{C_{chl}}$	HydroColor ratio used to estimate chlorophyll
CDOM	Chromophoric Dissolved Organic Material
$\mathbf{E_d}$	Downward Plane Irradiance (W m^{-2} nm^{-1})
$\mathbf{L_{rel}}$	Relative Radiance Measured By the Camera
$\mathbf{L_s}$	Sky Radiance (W m^{-2} sr^{-1} nm^{-1})
$\mathbf{L_t}$	Reference Surface Radiance (W m^{-2} sr^{-1} nm^{-1})
$\mathbf{L_w}$	Water Leaving Radiance (W m^{-2} sr^{-1} nm^{-1})
PAR	Photosynthetically Active Radiation
R	Irradiance Reflectance (%)
$\mathbf{R_{rs}}$	Above Water Remote Sensing Reflectance (sr^{-1})
$\mathbf{r_{rs}}$	Subsurface Remote Sensing Reflectance (sr^{-1})
RGB	Digital Value From the Camera's Red, Green, or Blue Channel
Tur	Turbidity (NTU)
$\boldsymbol{\alpha}$	Camera Exposure Time (s)
$\boldsymbol{\rho}$	Fraction of Sky Radiance Reflected by the Water Surface
$\boldsymbol{\theta}$	Zenith Angle (°)
$\boldsymbol{\phi}$	Azimuth Angle (°)

CHAPTER 1

INTRODUCTION

Due to the Earth's enormous coastal population, monitoring the water quality of coastal and inland water bodies is critical. Water quality, defined for the purposes of our study, is the chemical, physical, and biological condition of the water. This includes phytoplankton concentration, amount of suspended sediments, concentration of dissolved organic material, temperature, salinity, pH, and many more.

Many of these parameters have been measured optically using both in and above water methods. Numerous optical instruments such as fluorometers, scattering sensors, radiometers, and spectrophotometers have been used in water quality monitoring. However, these instruments are typically expensive and often require trained personnel to operate them. The high resolution and sensitivity of these instruments make them unnecessarily complicated for many coastal and inland monitoring applications.

The potential use of smartphones in water quality monitoring applications has been overlooked by the oceanographic and limnological community. This thesis details an investigation into whether a smartphone camera can be use as a water quality sensor. This proposition raises many interesting scientific questions. Can the camera be used to measure light intensity? What kind of spectral resolution does an off the shelf camera have? Can you relate the color perceived by the camera to the concentration and type of particles in the water? This thesis aims to answer these questions. The work presented here follows in the footsteps of two previous studies that attempted to measure water quality using a digital camera (Goddijn et al. 2009; Goddijn and White 2006). This study improves the methodology and

provides a more comprehensive measure of water quality. This work also represents the first attempt to distribute such algorithms via a smartphone platform.

1.1 Why Monitor Water Quality?

The global population continues to rise exponentially with no sign of slowing. Greater than half of the worlds 7 billion population live and work within 200 km of the coast (Hinrichsen 1999). Anthropogenic effects on the ocean due to this enormous coastal population are unavoidable. Some of the numerous impacts from the coastal population include: harmful algal blooms, coastal erosion, nutrient loading, and hypoxia. High resolution water quality datasets are the best method to assess the frequency and extent of these effects.

Water quality is not measured in an absolute sense. Each type of environment will have its own characteristic values for parameters like chlorophyll or suspended sediment concentration. It is the fluctuation or deviation from these typical values that is important. Large deviations from these values can be indicative of changes in the ecosystem. Therefore, the goal of monitoring is two-fold. It provides a time series that can be used to determine what conditions are typical of an environment, and it will detect deviations from these typical values.

Chlorophyll *a* (hereinafter referred to as simply chlorophyll) is one of the most widely measured water quality parameters. Chlorophyll can indicate the health of a coastal ecosystem by providing a proxy for the amount of phytoplankton in the water column. Large deviations from the average chlorophyll concentration can indicate a disruption in the environment, which can lead to shifts in the ecosystem (Boyer et al. 2009). High values are typically associated with high levels of nutrients (nitrates and phosphates), which in many cases are introduced to the coastal ocean by anthropogenic pollution (e.g. sewage, fertilizer). Extremely low values may indi-

cate oligotrophication due to acid rain or introduction of toxins to the environment (Kwiatkowski and Roff 1976).

The concentration of suspended sediments can provide useful information about sediment transport and underwater light propagation. Abnormally high concentrations of suspended sediments can indicate destabilization of terrestrial sediments. This could be caused by erosion, dredging activities, and/or coastal development. An increase in suspended sediment concentration will also decrease light for phytoplankton, potentially leading to lower primary production. Suspended sediments can also be important in the transport of adsorbed toxins or adsorbed organic material (Eggleton and Thomas 2004; Voice and Weber 1983).

1.2 Optical Properties of Chlorophyll, SPM, and CDOM

Chlorophyll, suspended sediments, and dissolved organic material all absorb and scatter light in a unique way. The interaction of these substances with light is well known and can be used to estimate the concentration of each substance. Simple optical algorithms have been, and continue to be, developed to measure these environmental indicators.

Chlorophyll, when combined with other cellular components has a broad absorption peak near 440nm and another smaller peak at 676nm. As a result of these absorption features, waters rich in chlorophyll will have a high reflectance in the green and a low reflectance in the blue (Clarke et al. 1970). Therefore, blue to green ratios have been used to measure chlorophyll concentration from reflectance (O'Reilly et al. 1998; Aiken et al. 1995).

Chromophoric dissolved organic material (CDOM) has a very predictable absorption spectrum. The spectrum exponentially decreases from blue to red with a slope of 0.01-0.02 nm^{-1} (Babin et al. 2003[a] ; Bricaud et al. 1981). Waters rich in

CDOM typically appear very dark, as result of CDOM absorbing in the blue-green wavelengths and water absorbing in the red wavelengths. In CDOM rich waters, it may be difficult to separate absorption from CDOM and absorption from chlorophyll in the blue portion of the spectrum.

Suspended sediments can typically be identified by their strong scattering properties. An increase in suspended sediment will cause water leaving radiance to increase over all wavelengths. The spectral dependence of the backscatter coefficient for mineral particles is generally modeled as a simple power law with a slope between 0-1 (Babin et al 2003[b]). To avoid the absorption bands of chlorophyll and CDOM, suspended sediments are typically measured by examining the magnitude of reflectance in the red and near infrared portions of the spectrum (Nechad et al. 2010).

1.3 Digital Cameras and RGB Values

Digital cameras use an array of charged coupled devices (CCDs) or complementary metal oxide semiconductors (CMOS) to collect high resolution light intensity data. Each detector in the array acts as a small light sensor (i.e. produces a voltage proportional to the amount of light incident on the detector). Black and white cameras consist of only this array and measure from no light (black) to saturating light (white). The amount of gray shades between black and white depends on the resolution of the sensor. Typical cameras have a resolution of 8 bits, corresponding to 256 possible values (2^8). A color camera is simply the same detector array covered by a Bayer filter. The Bayer filter has a repeating pattern of colored filter elements (figure 1.1). This provides spectral information in the form of large bands in the red, green, and blue portions of the visible spectrum. Using the amount of light measured by each detector, each pixel is assigned an red, green, and blue (RGB)

value between 0 and 255. The Bayer filter is transparent to infrared light, therefore cameras have an additional infrared filter to prevent infrared light from reaching the detector array.

A digital camera, while not designed to sense the surrounding environment in a quantitative way, can nonetheless be used to gain information about one's surroundings. The CCD or CMOS array, like all silicon based light sensors, generally have a linear response to light intensity. Therefore, each pixel of the camera can be used as a primitive radiometer. The bandwidth of the Bayer filter elements are wide and overlapping, however it is still possible to obtain spectral information.

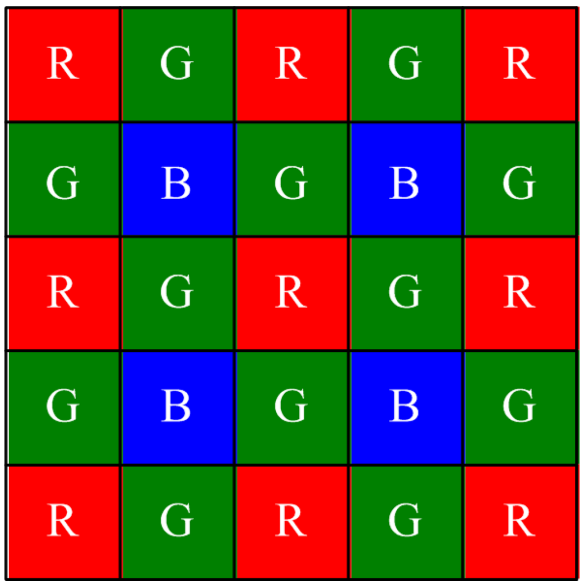

Figure 1.1. Bayer filter used in color cameras. Each filter covers a single detector in the cameras detector array.

1.4 Remote Sensing

In order to gather environmental data over large spatial scales, many scientific fields have adopted remote sensing. Remote sensing allows for rapid high resolution measurement of radiances or reflectances from the earth or sea surface. In oceanography, satellites are used to measure the radiance of light in visible and near

infrared that is leaving the top of the atmosphere. Additional data from meteorological satellites and various ancillary data are used to propagate the radiance leaving the atmosphere to the radiance leaving the sea surface (Lee et al. 2007; Gordon and Wang 1994). This data is also used to estimate the downward plane irradiance at the sea surface. These values are combined to provide a measure of the water reflectance, known as remote sensing reflectance (R_{rs}):

$$R_{rs}(\theta, \phi, \lambda) = \frac{L_w(\theta, \phi, \lambda)}{E_d(\lambda)} \tag{1.1}$$

Where θ and ϕ are the viewing zenith and azimuth angles, λ is wavelength, L_w is the water leaving radiance, and E_d is the downward plane irradiance. Remote sensing reflectance provides a nearly illumination independent measure of the waters reflectance.

Remote sensing reflectance is highly influenced by the absorption and scattering properties of water and the particles it contains. The optical properties of phytoplankton pigments (including chlorophyll) and suspended sediments (discussed in section 1.2) have a large influence on the shape and magnitude of R_{rs} (Gordon et al. 1988).

The use of satellites to measure R_{rs} is limited in coastal and inland waters. A single pixel from a satellite image has a large footprint on the surface of the earth. Therefore, a single pixel near the coast often contains radiance from both land and water. Spatial resolution of remote sensing images has been improved by measuring R_{rs} from aircraft. However, large scale collection of R_{rs} in coastal waters is a challenge. The smartphone application presented here has the potential to help supplement remote sensing data by collected measurements of R_{rs} in coastal areas inaccessible to satellites.

CHAPTER 2

THE IPOD AND IPHONE CAMERA

HydroColor was developed using an iPhone 4, iPhone 5 and an iPod touch. Each device contains a different camera, however, the general operation of the cameras follow the description in section 1.3. A series of laboratory tests was conducted to determine the camera's response to light intensity and its spectral sensitivity, the results of which are discussed in this chapter.

2.1 Specifications

Data collection and testing of HydroColor was conducted primarily on four Apple devices: iPod touch (4th generation), iPhone 4, and two separate iPhone 5 devices. All devices possessed a forward and backward facing camera. This study only makes use of the forward facing camera, thus any reference to the iPhone or iPod camera is referring to the forward facing camera. The fourth generation iPod contained a 0.7 megapixel color camera (720 x 960 pixels). The iPhone 4 contained a 5 megapixel color camera (2592 x 1936). The two iPhone 5 devices contained an 8 megapixel camera (2448 x 3264).

Apple imposes some limitations on how the camera can be controlled. The majority of camera settings can not be manually adjusted (e.g. focus, white balance, exposure time). The only way these values change is through inaccessible device software. However, the camera's settings can be locked on their current value. Therefore, it is possible to have some control over the camera settings without the ability to actually set them to a specific value. All images taken by each device were handled in the RGB color space.

2.2 Spectral Sensitivity

The spectral sensitivity of most color cameras is created by the Bayer filter used to cover the detector array. Bayer filters are explained in section 1.3. The sensitivity of most cameras are similar because the objective is to create an image that will reproduce colors as seen by the human eye (not necessarily the true color). The Bayer filter accomplishes this by creating three wide overlapping bands in the red, green, and blue portions of the visible spectrum. For the purposes of this study, only the relative sensitivity of each color channel needed to be known. Whether one channel is more sensitive than another is irrelevant because the comparison between channels occurs after taking a ratio where any amplification factor is canceled (assuming the channel is not saturated).

The spectral sensitivity of an iPod touch (4th generation), iPhone 4, and iPhone 5 were investigated. Each device was placed inside a Cary 50 UV-Vis spectrophotometer so the camera was viewing the variable light source. A sheet of tracing paper was placed over the camera to diffuse the direct beam from the spectrophotometer light source. A short script was created in Xcode which locked the white balance and exposure on the camera and recorded the RGB values once per second. The spectrophotometer was set to scan from 800 to 300nm. While the scan proceeded, the script to record the RGB values was run on the device. A baseline reading of the spectrophotometer light source with the sample chamber empty provided the relative intensity of the light source (which was variable over the 800 to 300nm scan). Each sensitivity curve was divided by the baseline in order to account for the variability in the light source intensity. The sensitivities curves were then smoothed using a 20nm moving average. Finally the curves were normalized by the highest recorded value for each channel.

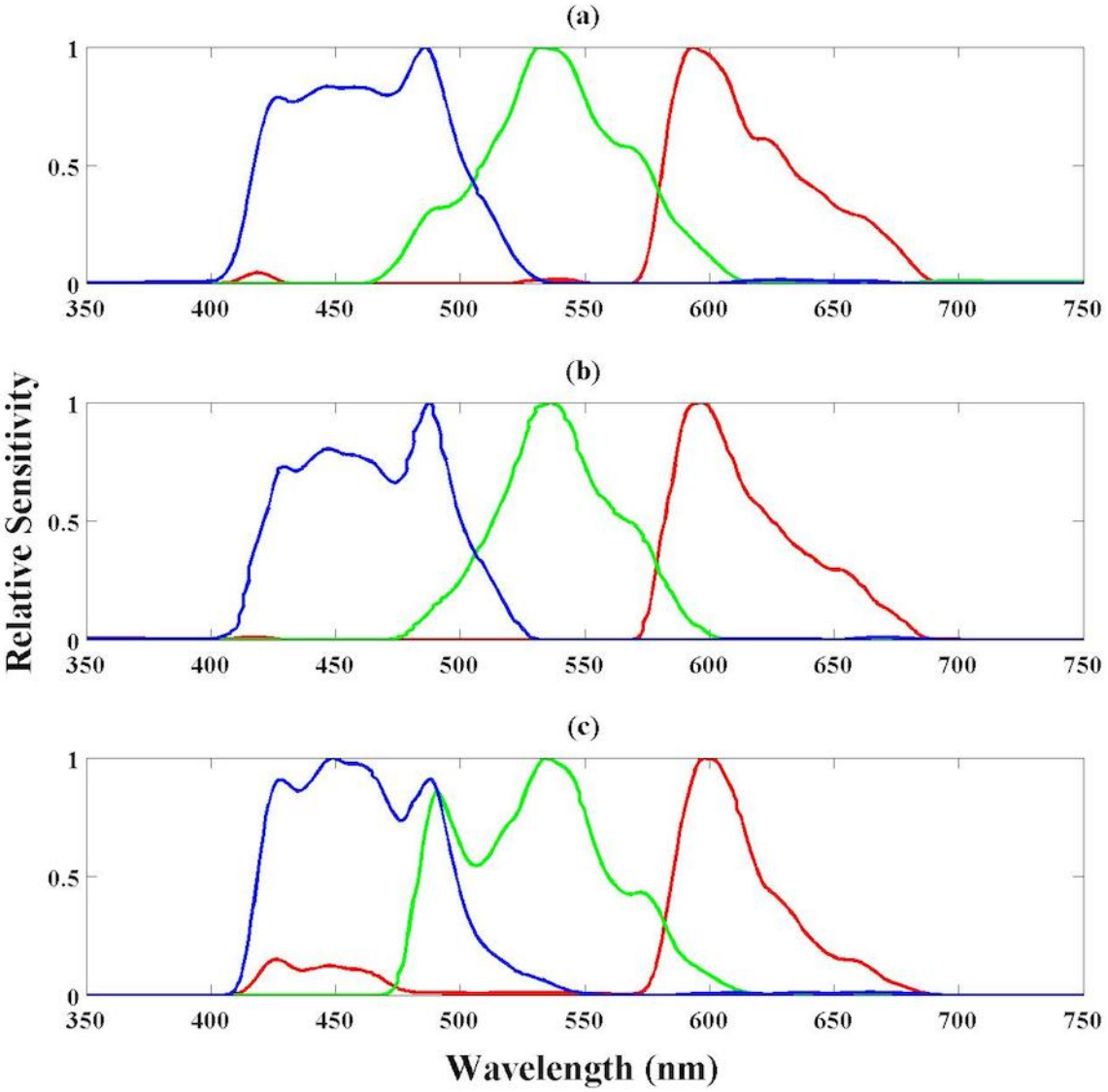

Figure 2.1. Spectral Sensitivity curves for the iPod Touch (a), iPhone 4 (b), and iPhone 5 (c). Spectral sensitivities were determined by viewing a spectrophotometer light source with each device. The camera exposure time and white balance were held constant during data collection. Each curve was smoothed using a 20nm moving average, then normalized by the highest recorded value.

The sensitivity curves where similar across all three devices (figure 2.1). In total the three color channels cover the visible spectrum from approximately 410 to 690nm. The iPod touch and iPhone 4 both had very similar spectral sensitivity in all channels. The iPhone 5 slightly departs from the iPod touch and iPhone 4

Table 2.1. Attributes of the iPod Touch, iPhone 4 and iPhone 5 color channel sensitivity curves. The wavelength of maximum sensitivity and the full width at half maximum (FWHM) of each curve is reported.

Parameter	iPod	iPhone 4	iPhone 5
Peak Red (nm)	593	597	598
FWHM Red (nm)	51	44	35
Peak Green (nm)	532	536	534
FWHM Green (nm)	66	54	77
Peak Blue (nm)	486	488	449
FWHM Blue (nm)	85	79	79

in the green and red sensitivity. The iPhone 5 green sensitivity curve possess an additional peak at 490nm that is not present in the iPod touch or iPhone 4. The iPhone 5 also has higher sensitivity to blue light in the red channel. In general, the peaks of the sensitivity curves are very similar for each device. However, the width of the peaks appear more variable (table 2.1). The spectral sensitivity curves of a second iPhone 5 were also measured. The peak location and peak widths were not significantly different from the iPhone 5 curves shown in figure 2.1.

The spectral response curves were reasonable in comparison to another study that preformed similar tests. Goddijn-Murphy et al. (2009) used a similar method to investigate the spectral response of a Nikon Coolpix885 and a SeaLife ECOshot. The position of the peak wavelengths were similar, however, the width at half max measured in this study were generally smaller than what is reported by Goddijn-Murphy et al. (2009). Additionally, the flat peak of the blue curve seen in this study was not present in the Coolpix885 or SeaLife ECOshot curves. Therefore, the Bayer filters used in these devices are slightly different.

2.3 Response to Light

The basic function of the detector array (CCD or CMOS) is to the measure light intensity. While the digital values of an RGB image vary between 0-255 as a function of light intensity, the exposure time of the camera is also variable. A long exposure time is an indicator of low light conditions and vise versa. Therefore, both the RGB values and exposure time must be accounted for when relating camera output to light intensity. The RGB value should be proportional to light intensity and the exposure time inversely proportional. Thus, to get a measure of relative radiance the following equation is used:

$$L_{rel} = \frac{RGB}{\alpha} \tag{2.1}$$

Where L_{rel} is the relative radiance measured by the camera, RGB is the red, green, or blue digital values returned by the camera, and α is the exposure time.

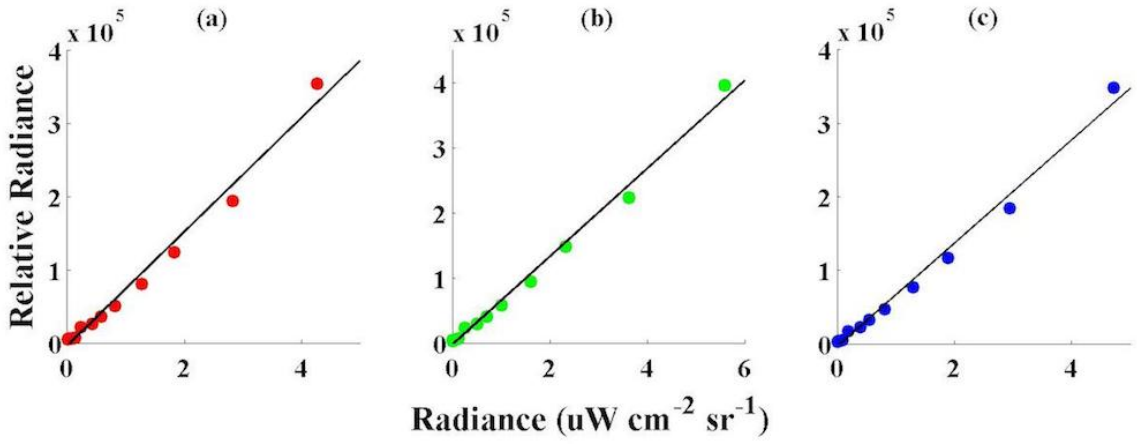

Figure 2.2. Camera response as a function of radiance. Measurements were made by gradually attenuating a white light source while collecting images with an iPod touch. The response in the red (a), green (b), and blue (c) color channels are shown. This figure is meant to show the linear relationship between normalized RGB values and radiance, it is not meant to provide an absolute calibration for measuring radiance.

The relationship between the cameras measure of relative radiance and actual radiance was investigated in the lab. An iPod touch was used to take images of a

diffuse light source that was gradually attenuated. A Satlantic radiometer was used to simultaneously measure the radiance of the diffuse light source. The hyperspectral radiance spectra were averaged using the iPod sensitivity curves in figure 2.1 as weights. The relationship between the camera's measure of relative radiance and the true radiance was linear (figure 2.2). The results of this investigation simply show the linear response of the cameras measure of relative radiance to the true radiance. This is not meant as an absolute calibration of the camera. The slope of the lines in figure 2.2 are likely to change with cleanliness of lens, temperature, age, and device type.

The dark current for the camera on all devices was negligible. Even if the exposure time was large, the RGB values of a completely black image were typically less then 3 counts. Therefore, the subtraction of a dark measurement was not necessary. This is confirmed by the near zero y-intercepts in figures 2.2, 4.7, and 4.8.

CHAPTER 3

RGB TO R_{RS}

This chapter will discuss how HydroColor is able to calculate the remote sensing reflectance from three images. The first few sections will explain the how the three images are collected. The last section will explain how these images can be converted into the remote sensing reflectance.

3.1 Water Leaving Radiance

Water leaving radiance L_w is defined as the radiance of light emanating from the water surface. A surface viewing radiometer will not provide a measurement of water leaving radiance. Radiance from the water surface will be a combination of the light emanating through the surface of the water and surface reflection (referred to as L_t). Thus, water leaving radiance is typically a calculated value rather than a measured one (with some exemptions: Lee et al. 2013).

In order to get a measure of the water leaving radiance using the camera, it will require two images. The first is an image of the water surface and the second is an image of the sky. The sky image is used to correct the water image for surface skylight reflection. Collection of the sky image is discussed in the next section.

Even though surface reflection cannot be eliminated, it can be significantly reduced by collecting the water image at a specific angle to the sun. An azimuth angle of 135° from the sun and an zenith angle of 40° from nadir are the optimum angles to minimize surface reflection (Mobley 1999). By taking advantage of the iPhone clock, GPS, compass, and gyroscope, a water image at these specific angles can be collected with ease.

HydroColor uses the current GPS coordinates and the Greenwich Mean Time (GMT) to determine the position of the sun in the sky. HydroColor puts this information into a simple sun model that runs onboard the phone. The sun model starts by solving the equation of time:

$$EoT = 9.87sin(2B) - 7.53cos(B) - 1.5sin(B) \tag{3.1}$$

Where B is equal to:

$$B = \frac{360}{365}(d - 81) \tag{3.2}$$

Where d is the number of days since the start of the year. The equation of time corrects both for the eccentricity of the Earth's orbit and for the Earth's axial tilt. Next a time correction (TC) factor must be calculated:

$$TC = 4Lon + EoT \tag{3.3}$$

Where Lon is the users longitude. The factor of 4 comes from the fact that the earth rotates 1° every 4 minutes. Using the time correction factor, the local solar time (LST) is calculated:

$$LST = T_{GMT} + \frac{TC}{60} \tag{3.4}$$

Where T_{GMT} is current GMT time in decimal hours. Using the LST, the hour angle (HR) is calculated:

$$HR = 15(LST - 12) \tag{3.5}$$

The hour angle is the angle of sun in the sky relative to solar noon (12 local time). The factor of 15, again, comes from the fact that the earth rotates 15° degrees per hour. Finally the sun's zenith (Ze) and azimuth (Az) angles can be calculated:

$$Ze = sin^{-1}(sin(\delta)sin(Lat) + cos(\delta)cos(Lat)cos(HR)) \tag{3.6}$$

$$Az = cos^{-1}\left(\frac{sin(\delta)cos(Lat) - cos(\delta)sin(Lat)cos(HR)}{cos(Ze)}\right) \tag{3.7}$$

Where Lat is equal to the users latitude and δ is equal to:

$$\delta = 23.45sin(B) \tag{3.8}$$

The azimuth angle provided by the above equation is in reference to true north, however the iPhone compass provides magnetic north. Therefore, HydroColor uses a look up table of declination values based on the users latitude and longitude and then interpolate to the correct magnetic declination value. The table comes from NOAA's National Geophysical Data Center and is hard coded into HydroColor. Newer iPhones do have an internal function that will adjust the compass to point to true north, however, I choose to do the calculation myself to ensure accuracy and usability for older devices. The lookup table only goes to $\pm 80°$ latitude. So I display a warning message indicating the sun model is not defined if the users is above or below 80 degrees (not likely).

The combined accuracy of the sun model and declination table was tested in comparison to software provided by the U.S. Department of Energy. A MatLab script accurate to $\pm 0.0003°$ was used to determined the true sun angles (Reda and Andreas 2008). The sun model described above, implemented on an iPhone, was accurate to within a few degrees of the true values. An error of a few degrees is negligible for the purposes of this study.

HydroColor uses the resulting azimuth angle to create the compass display. Two indicator arrows are rotated around a compass display so that when the north arrow is aligned with an indicator arrow, the phone is $\pm 135°$ from the sun. The zenith angle is not used, however, it is saved along with the rest of the data. It can be used later for quality control.

The gyroscope measures pitch, yaw, and roll of the phone. HydroColor uses the pitch and roll function to create an inclinometer display alongside the compass display. When the inclinometer display is aligned with two green arrows, the optical

axis of the camera is either 40 or 130° from nadir (40° for the water image and 130° for the sky image).

3.2 Sky Radiance

As alluded to in the previous section the water image must be corrected for skylight reflection off the surface of the water. The intensity and spectral signature of the skylight can be measured by collecting an image of the sky directly above the water image (sky radiance will be referred to as L_s). HydroColor uses the same sun model, compass display, and inclinometer to direct users to correct angles to take the sky image. Again, the sky image should be taken at ±135° from the plane of the sun. The pitch angle of the phone should be 90° from the angle at which the water image was taken, or 130° from the nadir. At this angle, the camera is viewing the portion of the sky that contributes the most to the surface reflection (Mobley 1999).

3.3 Downward Plane Irradiance

To measure the downward plane irradiance (E_d) HydroColor uses an image of a photographers gray card. A gray card is simply a piece of cardboard with a coating that reflects 18% of incident light. This is not the first study to use gray cards as reflectance standards (Briones and Aguilera 2005; Tole et al. 2000; Carder and Steward 1985). Gray cards, for the purposes of this study, can be assumed to be lambertian reflectors (Soffer et al. 1995) with a flat reflectance spectrum (Figure 3.1). Therefore, the radiance emanating from the gray card (L_c) is directly related to E_d. I chose gray cards as a reflectance standard because they are reasonably cheap and widely available (as opposed to Spectralon reflectance standards that are hundreds of dollars).

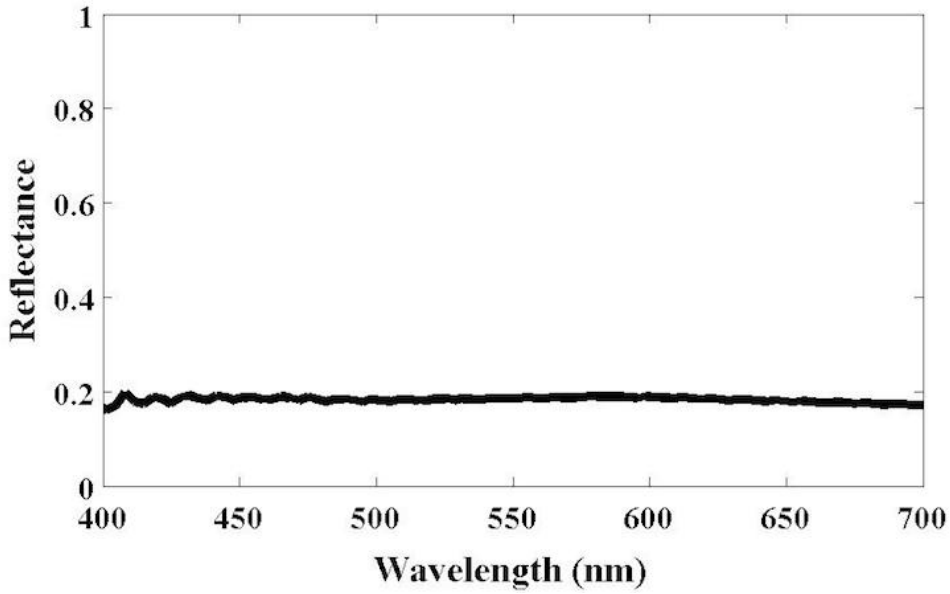

Figure 3.1. Reflectance of a Kodak gray card. Reflectance of the gray card was measured using a hyperspectral radiometer and referenced to a Spectralon plaque (95% reflectance) under the same illumination conditions.

Users are directed to take the gray card image at the same zenith and azimuth angles as the water image (135° from the sun and 40° from nadir). The angle of the gray card image is not critical since the gray card is a lambertian reflector. However, requiring users to take the image at this angle has a few advantages. The first is that specular reflection from the sun will not contaminate the image at this angle. The second is that when taking the gray card and water images, the users body will block a small portion of the sky radiance. If the two images are taken at the same angle, the hope is that the user will block the same portion of sky for both images.

3.4 Calculation of the Remote Sensing Reflectance

For each image, the RGB values from a 200x200 pixel square at the center of the image were averaged. The average values were then used to calculate the relative radiance using Eq. 2.1. Averaging over a large amount of pixels helps to reduce

noise in the image and account for variability in the image. Under clear sky or overcast conditions the images are very uniform in intensity (figure 3.2; figure 3.3). If there are patchy clouds, the intensity of the sky and water images can be variable (figure 3.4). Averaging helps to account for some this variability as opposed to using a single pixel.

The remote sensing reflectance (R_{rs}) is calculated by using the relative radiances measured by each image. The same formula used for precision radiometers can be applied to the camera measured radiances (Mobley 1999):

$$R_{rs} = \frac{L_t - \rho L_s}{\frac{\pi}{R_{ref}} L_c} \tag{3.9}$$

Where L_t is the radiance of the water surface, L_s is the sky radiance, L_c is the gray card radiance, R_{ref} is the reflectance of a reflectance standard, and ρ is the theoretical fraction of skylight reflected by the water surface. When calculating R_{rs} using the camera L_t, L_s, and L_c are replaced by the respective L_{rel} values from Eq. 2.1. The reference standard is the gray card which has a reflectance of 18% ($R_{ref} = 0.18$).

The benefit of using Eq. 3.9 is that any multiplicative error or scaling factor is canceled out in the equation. Therefore, the camera needs no absolute calibration. All that is needed to calculate R_{rs} is a quantity proportional to radiance. Indeed, the proportionality between radiance and the cameras measure of relative radiance is likely to change with cleanliness of the lens, age, temperature, and device manufacturer. However, because the images are all taken using the same device in a short period of time, these drift errors should cancel.

The value for ρ can be determined using HydroLight, which is a radiative transfer software used for determining above and below water radiance distributions. For the angles used to capture the water image (135° from the sun and 40° from the horizontal), and under ideal conditions, the value of ρ is approximately 0.028 (Mob-

ley 1999). For sun zenith angles greater than approximately 15°, ρ is independent of wavelength. The value of ρ can vary spectrally when there is large contribution from sun glint on the surface. This can occur when the sun zenith angle is less than 10° (figure 3.5). For the latitudes this study was conducted at, the sun zenith angle is never less than 10°. The sun zenith angle can reach values of less than 10° for latitudes between 25° N and 25° S.

Sea state (which is a function of wind speed) can have a large effect on the value of ρ. When the surface of the water is sloped, an observer or detector is viewing a different portion of the sky than what is seen on a level surface. Currently HydroColor does not obtain any information on wind speed or sea state. Therefore, this is a known source of error in the calculation of R_{rs}. The sensitivity of ρ on wind speed is a function of sun zenith angle and sky condition. As the sun is higher in sky, the influence of wind speed on ρ becomes greater. At a sun zenith angle of 30° degrees and a wind speed of 15 m s^{-1}, ρ can be as large as 0.05. This can lead to substantial error in R_{rs}. Therefore, it follows that HydroColor should not be used in high wind areas where the sea surface is choppy. Perhaps in the future HydroColor will access weather information via the iPhones data connection, however, for purposes of this study, the value of ρ is assumed to be invariant and is set to 0.028 in the HydroColor software. This is an accurate value of ρ for wind speeds less then 5 m s^{-1}.

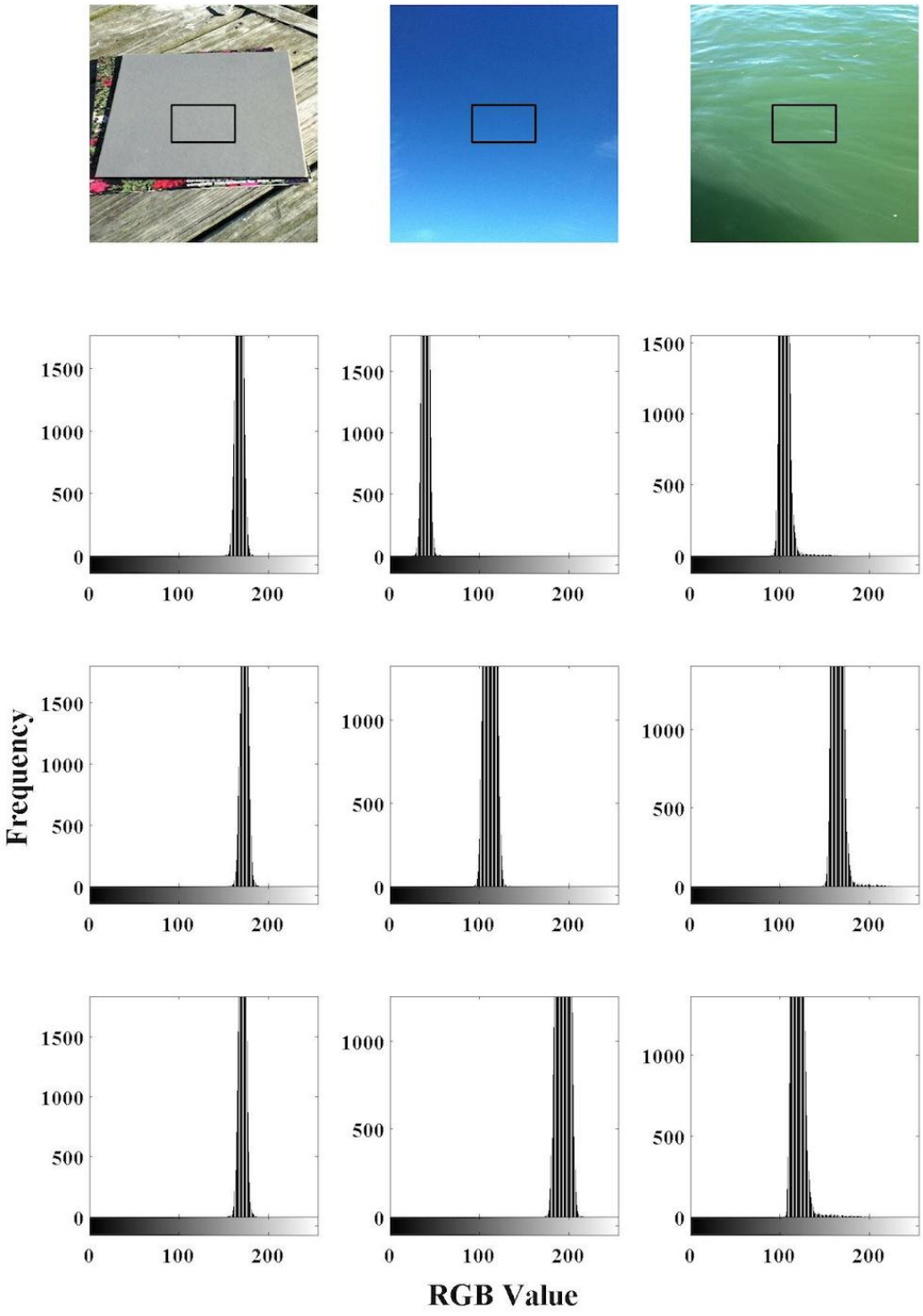

Figure 3.2. Histograms of RGB values for HydroColor images taken on a clear day. The black box in the first row of images shows the region used to generate the histograms below. The histograms show the frequency of RGB values for the red channel (row 1), green channel (row 2), and the blue channel (row 3).

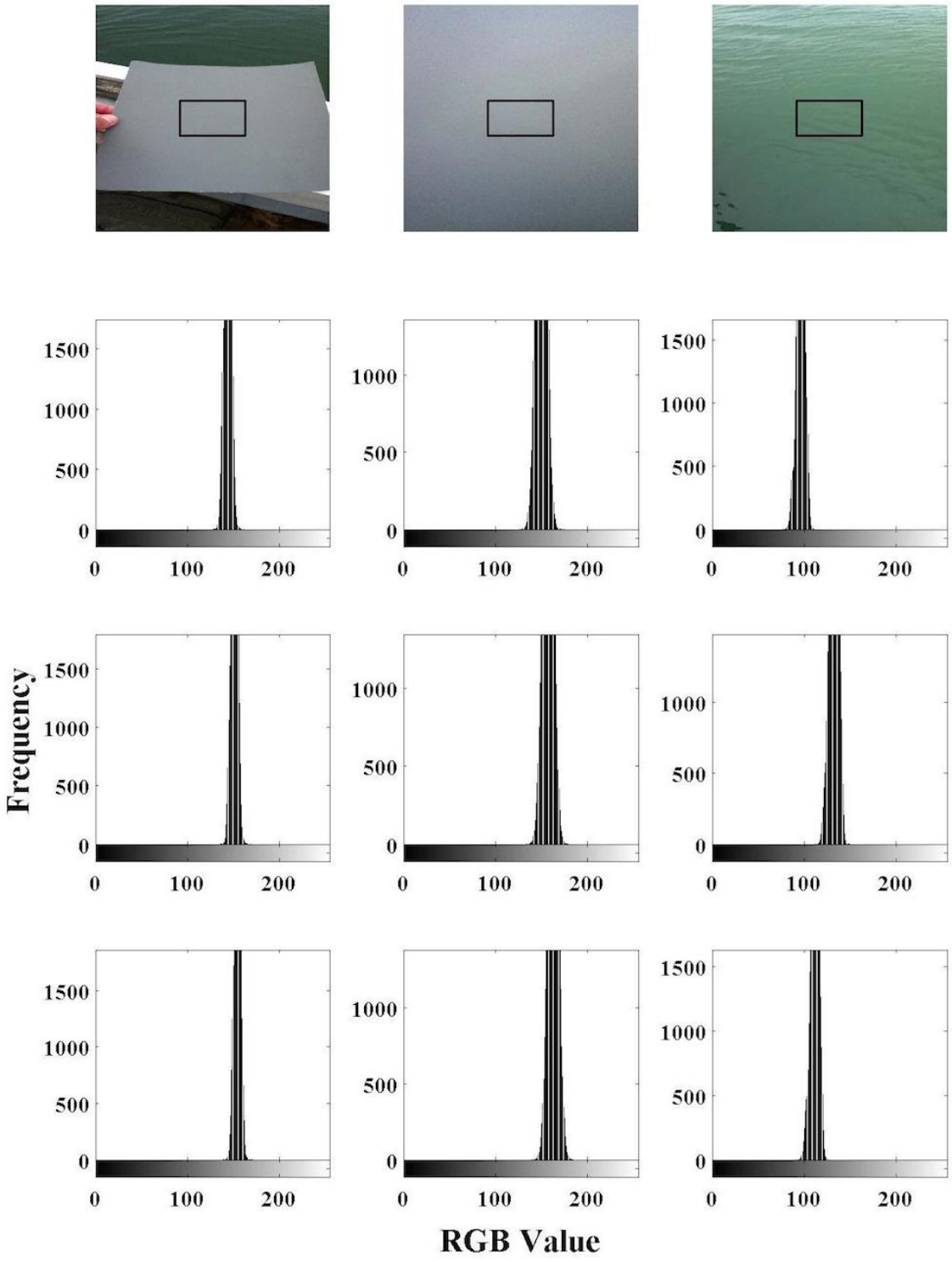

Figure 3.3. Histograms of RGB values for HydroColor images taken on an overcast day. The black box in the first row of images shows the region used to generate the histograms below. The histograms show the frequency of RGB values for the red channel (row 1), green channel (row 2), and the blue channel (row 3).

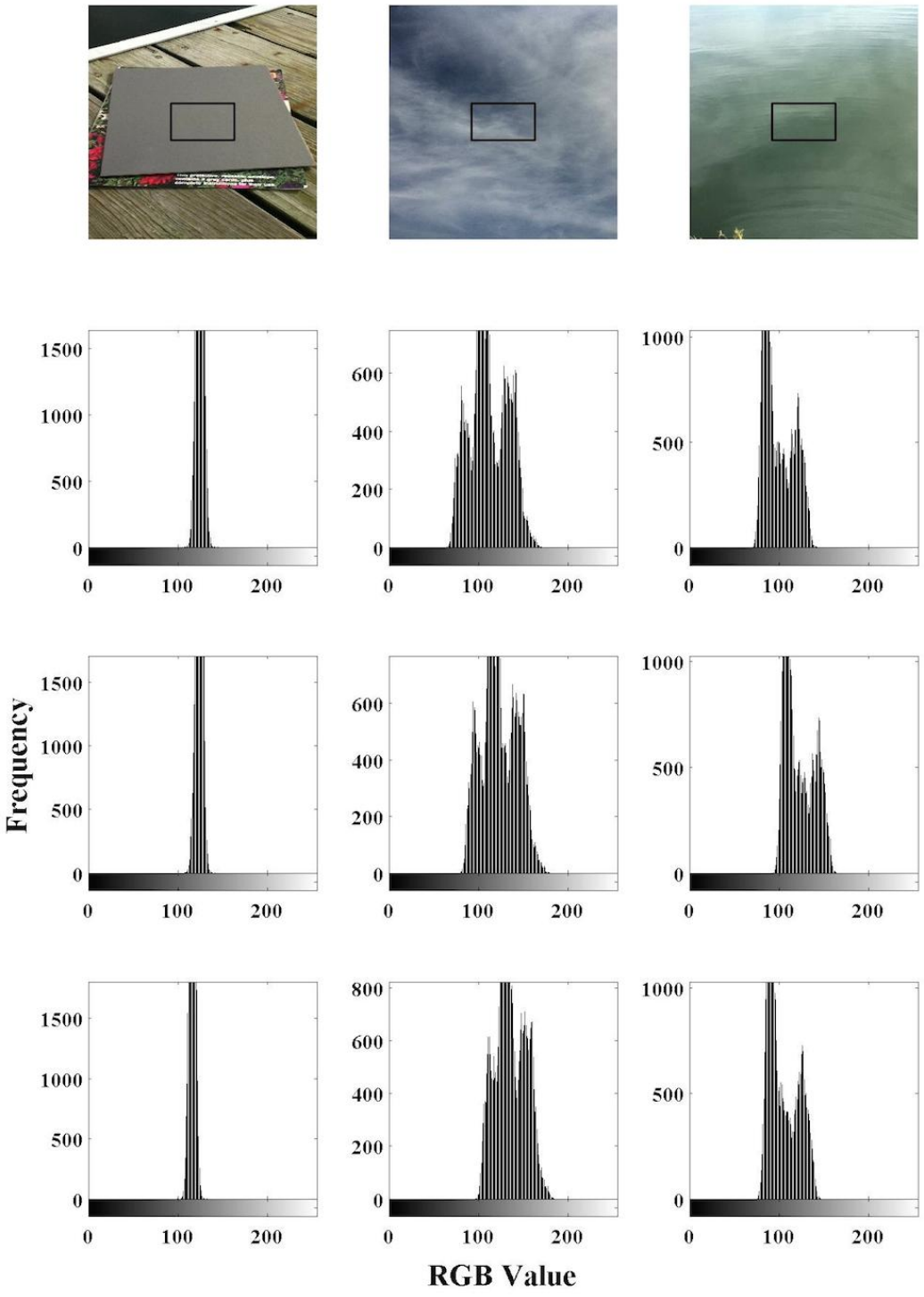

Figure 3.4. Histograms of RGB values for HydroColor images taken on a partly cloudy day. The black box in the first row of images shows the region used to generate the histograms below. The histograms show the frequency of RGB values for the red channel (row 1), green channel (row 2), and the blue channel (row 3).

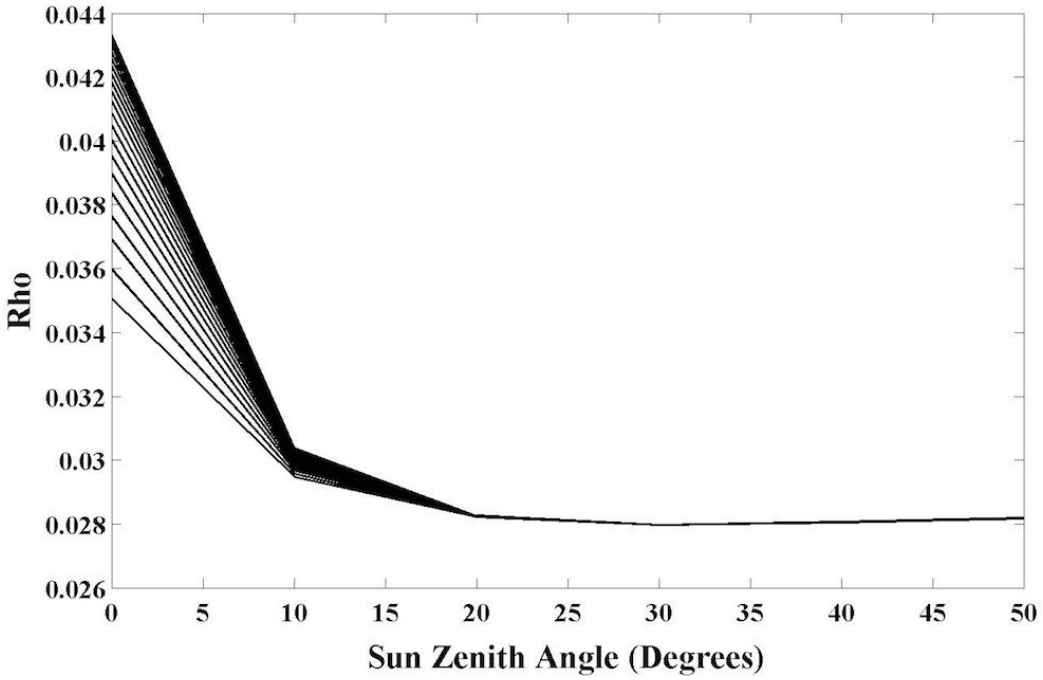

Figure 3.5. Reflectance factor as function of sun angle and wavelength. This figure shows the value ρ from 360-740nm at 20nm increments (360nm being the lowest line and 740nm being the highest, with all other wavelengths falling in-between). Values of ρ were determined using HydroLight with a clear sky and zero wind speed. For very high sun angles ρ not only increases, but becomes spectrally dependent. For sun zenith angles greater than 20°, the value of ρ is approximately 0.028 and is independent of wavelength or sun angle.

CHAPTER 4

FIELD TESTS

4.1 Overview of Sampling Locations

Field data were collected at 5 primary geographic regions: the mouth of the Columbia River, the coast of Maine, the Arctic Ocean, the coast of Georgia, and Quebec City (figure 4.1). HydroColor data was collected in parallel with a variety of other optical measurements. The concurrent data was used to validate HyrdoColor's calculation of R_{rs} and provide a calibration for the measurement of turbidity and chlorophyll.

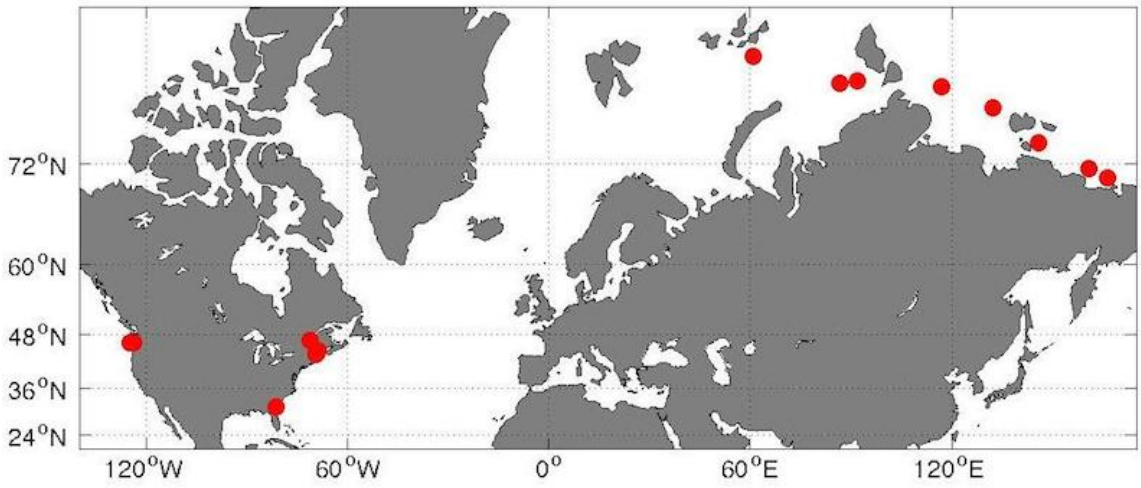

Figure 4.1. Overview of sampling locations.

4.1.1 Columbia River, OR, USA

Data were collected at the mouth of the Columbia River on the boarder of Oregon and Washington (figure 4.2). Data collection was in conjunction with the Office of Naval Research study: RIVET-II. Data were collected over a period of five

days onboard the R/V Point Sur (6/1/13 - 6/5/13). Images were collected by Dr. Emmanuel Boss, running HydroColor on an iPhone 5. Both HydroColor and Water Insight Spectrometer (WISP) measurement were collected at 34 different sites. Both dissolved and particulate absorption and attenuation measurements were collected using a WetLabs AC-s. The AC-s was mounted onboard a profiling optical package. Sky conditions over the 5 days ranged from overcast, to patchy sun and clouds, to clear skies.

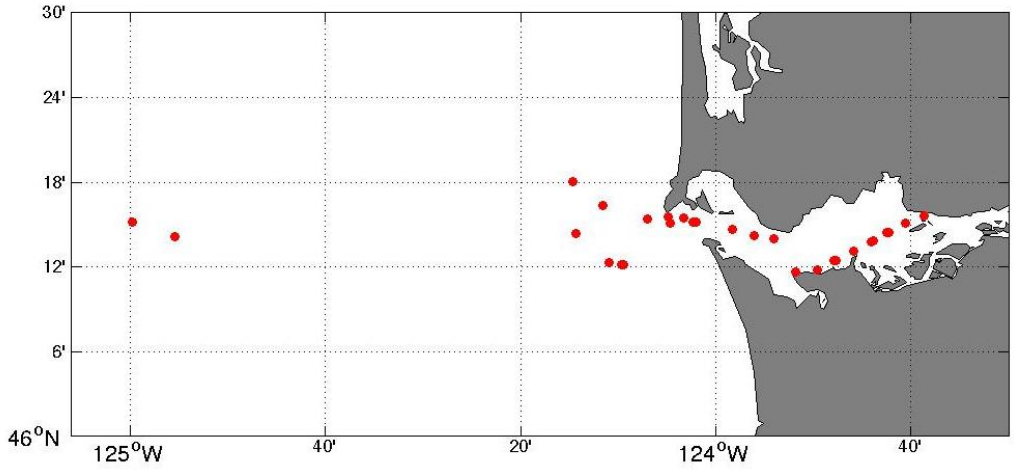

Figure 4.2. Map of Columbia River sampling stations. Data were collected at these points over a period of five days aboard the R/V Point Sur.

4.1.2 Coastal Maine, USA

Data were collected along the coast of Maine during two field campaigns. The first was during the 2013 summer course: Calibration and Validation for Ocean Color Remote Sensing. The course was held at the Darling Marine Center (DMC) in Walpole, ME. The DMC is located along the Damariscotta River Estuary, which is a highly productive estuary that extends several miles inland. During the summer course at the DMC, two cruises on board the R/V Ira C were conducted on 07/22/14 and 07/24/14. Both cruises transected the lower half of the estuary. The cruise on

7/22/14 conducted an additional offshore station approximately a mile from the mouth of the estuary.

Two full sampling stations were conducted during each cruise, one inside the estuary and the other conducted either at the mouth of the estuary or offshore. At each station, radiometric data was collected using both in-water and above water radiometers. In water radiance measurement were conducted using a Satlantic HyperPRO in buoy mode. Above water radiance measurements were collected using both a Satlantic HyperSAS and a WISP. Multiple profiles were taken using an optical package that contained an AC-s, b_b-9, and a chlorophyll fluorometer. Water samples were collected at the surface and at 4m for CDOM and chlorophyll analysis in the lab. At end of each cruise, collected water samples were filtered through GFF filters. Absorbance of the filtrate was measured on Cary 50 UV-Vis spectrophotometer to determine CDOM absorption. Chlorophyll concentration was measured using extraction and fluorescence measurement follow the JGOFS protocol (Knap et al. 1996).

Images were collected using HydroColor at each of the stations. Between full stations, multiple short stations were conducted. Short stations consisted of above water radiometric measurements along with images collected using HydroColor. During the first cruise on 07/22/14, HydroColor images were collected by classmate Grace Kim using an iPhone 5. During the second cruise, HydroColor data was collected on both an iPhone 5 and an iPod touch. Sky conditions for the first cruise were patchy sun and clouds. Sky conditions for the second cruise were fully overcast (slightly foggy), eventually giving way to patches of sun and clouds.

The second round of data collection in Maine consisted of 12 sampling sites at 12 different docks from Bangor, ME to Waldoboro, ME (figure 4.3). All 12 sites were sampled on 10/10/13. At each site, three replicate above water radiance measurements were collected using a WISP. Turbidity was measured using a Hach

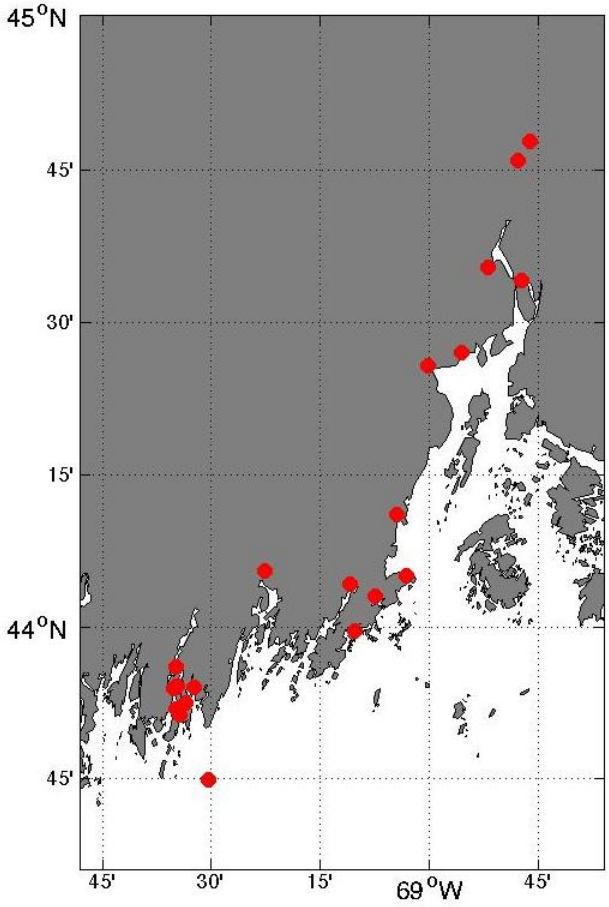

Figure 4.3. Map of sampling locations along the coast of Maine. Points clustered in the lower left are from data collected during two cruises aboard the R/V Ira C. The rest of the data were collected from various docks located along the coast between Bangor, ME and Waldoboro, ME.

2100Q turbidimeter. One water sample was collected and its turbidity was measured three times using the turbidimeter, inverting the sample between measurements. Images were collected using HydroColor running on an iPod touch. Six replicate sets of images were collected per site. Sky conditions were mostly sunny, with passing clouds.

4.1.3 Arctic Ocean

Three HydroColor images sets were collected onboard the R/V Tara during the Tara Ocean Polar Circle expedition. Images were collected using HydroColor run-

ning on an iPod touch. Continuous optical data was recorded along the majority of the expedition. Notable optical measurements made concurrently with HydroColor measurements are: absorption and attenuation measured by an AC-s, backscatter measured by a b_b-3, and CDOM absorption measured by an UltraPath.

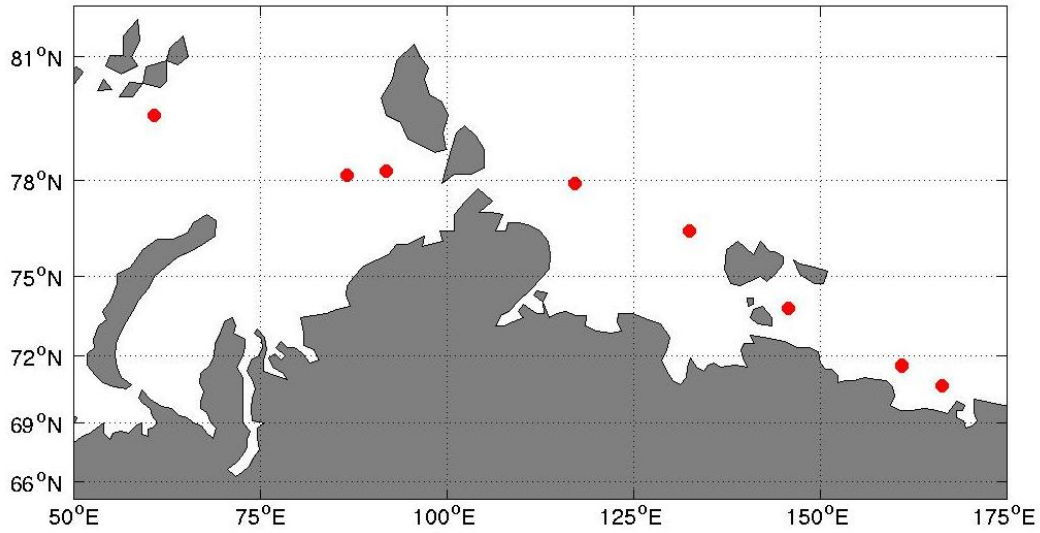

Figure 4.4. Map of sampling locations in the Arctic Ocean. Only the three westernmost points were collected using the HydroColor software. The rest of the data points were collected using an iPod touch camera as-is.

During the cruise, the apple developer's license for the device running HydroColor expired. Only data from the Kara Sea was collected using HydroColor (figure 4.4). The rest of the data points are where images were collected using the iPod camera as-is. This is not ideal because there is no control over the white balance of the camera. The exposure times for the non-HydroColor images were retrievable from the image EXIF data. Data not collected using the HydroColor software was excluded from the analysis, however, some of the data proved useful for exploring the cameras ability to measure photosynthetically active radiation (section 4.5).

4.1.4 Coastal Georgia, USA

Data were collected on 9/28/13 along the midcoast of Georgia inside Sapelo Sound and in the neighboring salt mash creeks (figure 4.5). Sapelo Sound is surrounded by salt marshes, which leads high levels of both dissolved and particulate organic matter. The benthos is also made up of silt, which leads to high levels of suspended sediment. Data from this region provided all the turbidity values higher than approximately 10 NTU in the data set.

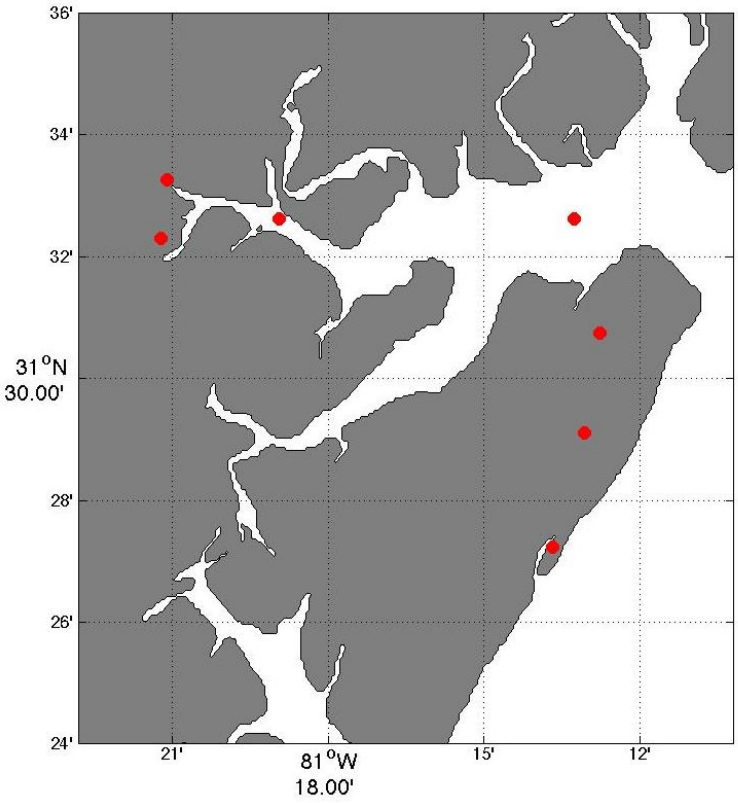

Figure 4.5. Map of sampling locations along the coast of Georgia. Data points that appear over land are inside a narrow salt marsh creek.

The method for data collection was very similar for the coastal Maine measurements. Both a WISP and Hach 2100Q where used to collect radiance and turbidity data at 7 different sites in and around Sapelo Sound. Images were collected using HydroColor running on both an iPod touch and an iPhone 4. Two replicate sets of

images were collected on each device per sampling site. Sky conditions were mostly sunny.

4.1.5 Quebec City, Canada

One round of sampling of was conducted at the Quebec City port on the St. Lawrence river on 11/12/13. Three replicate sets of images were collected running HydroColor on an iPod touch. Three replicate turbidity measurements were made on the same water sample using the Hach 2100Q turbidimeter. Sky conditions were sunny with light clouds.

4.2 R_{rs} Comparison

The majority of HydroColor data collected in the field were accompanied by WISP measurements. Both HydroColor and the WISP are designed to measure R_{rs} using the same method. The WISP uses three spectrometers to measure L_t, L_s, and E_d. Therefore, the WISP served as a convenient instrument to determine the accuracy of HydroColor.

After collecting a significant amount of data with WISP, it became apparent the WISP measurement of R_{rs} was incorrect. A comparison of in-situ WISP and HyperSAS measurements of R_{rs} showed that the WISP consistently underestimated R_{rs}. This was confirmed by examining a dataset of concurrent WISP and HyperSAS measurements during a cruise in the Atlantic (data provide to me by Dr. Ivona Cetinic). To correct the error in the WISP measurement of R_{rs}, a vicarious calibration was preformed between the three spectrometers of the WISP and a recently calibrated Satlantic radiometer and irradiometer. In a dark room, a 95% reflectance Spectralon plaque was illuminated with incandescent and LED lights (which provided a large amount of light between 450 and 700nm). Measurements were collected of the plaques radiance using the Satlantic radiometer and then with the WISP's L_t and

L_s spectrometers. The plaques irradiance was then measured using a Satlantic irradiometer, then with the WISP's E_d spectrometer. The ratio between the Satlantic measurements and the WISP measurements provided the calibration for each of the WISP's three spectrometers (figure 4.6). Inaccuracies in the WISP spectrometers have been found in pervious studies, and were handled similarly (Hommersom et al. 2012). Any subsequent reference to WISP measurements are referring to WISP data after the vicarious calibration has been applied.

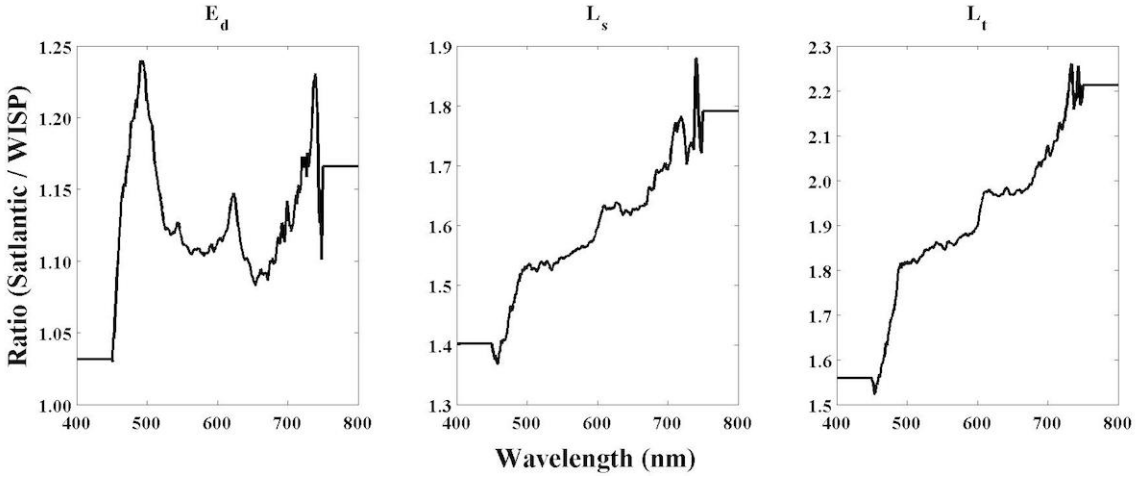

Figure 4.6. Vicarious calibration of the WISP. The three graphs display the ratio of radiance or irradiance measured by a Satlantic radiometer to the radiance or irradiance measured by the WISP. E_d, L_s, and L_t refer to the different spectrometers on the WISP. Low light levels or noise caused erroneous values in the very short and very long wavelengths, therefore the ratio is assigned a constant value for these regions.

After the vicarious calibration was applied, R_{rs} was calculated using Eq. 3.9. In order to compare the WISP hyperspectral R_{rs} with HydroColor R_{rs}, the WISP spectra where averaged using the spectral sensitive curves in figure 2.1 as weights. For each color channel, a regression line was fit to the WISP and HydroColor R_{rs} using type-I linear regression. Three outliers were removed using an iterative fitting process. After the initial fit, the standard deviation of the absolute error between the model predicted values and the measured values was calculated. Any data falling

more then 3.5 standard deviations outside the mean fit error were removed. The function was then fit to the data set that no longer contained the outliers.

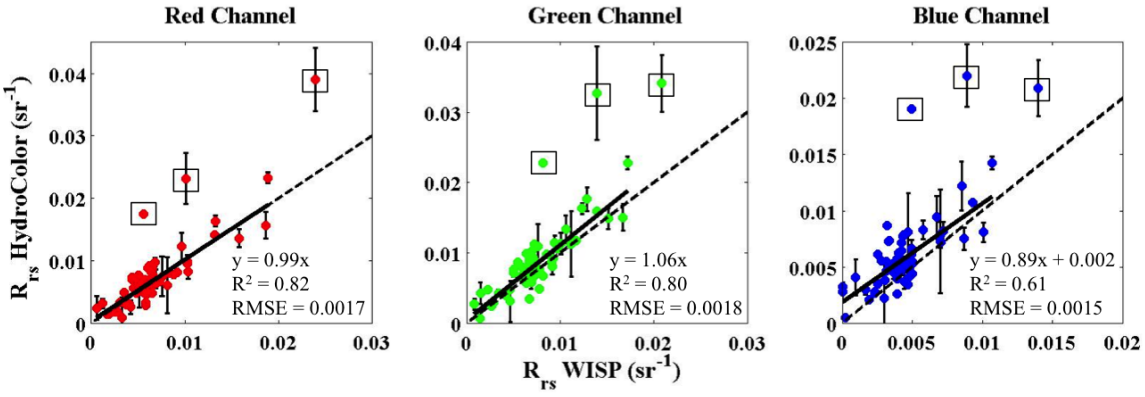

Figure 4.7. Comparison of HydroColor R_{rs} with WISP R_{rs}. The three plots show the R_{rs} comparison for each color channel. In order to show a meaningful comparison, the WISP spectra were averaged using the camera spectral sensitivity curves as weights. Error bars display the standard error, when available. The dashed line shows the one to one line and the solid line shows the results of a type-I linear regression. The data points in boxes were identified as outliners and were not included in the regression.

The HyrdoColor measured R_{rs} compares well with the concurrent WISP measurements (figure 4.7). The majority of data points fall along the one to one line. The scatter of the data around the one to one line is similar for all channels (note the difference in scale for the blue channel in figure 4.7). The range of R_{rs} values spanned in the data set is significant, however, HydroColor has yet to be tested in very turbid waters. The median percent error in of the HydroColor measurement of R_{rs} relative to the WISP was 18%, 16%, and 26% for the red, green, and blue channels respectively. The error in ρ is not realized in this comparison because the same value of ρ is used for both the HydroColor and WISP calculations of R_{rs}. If there is a large error in ρ it will appear in the comparison of HydroColor R_{rs} with the modeled value of R_{rs} (next section).

There are a number of occurrences that may have generated the three outliers seen in figure 4.7. The speed at which images are collected may play an important role, especially when there are patchy clouds. If the illumination or sky conditions change between images, it would lead to incorrect R_{rs} values.

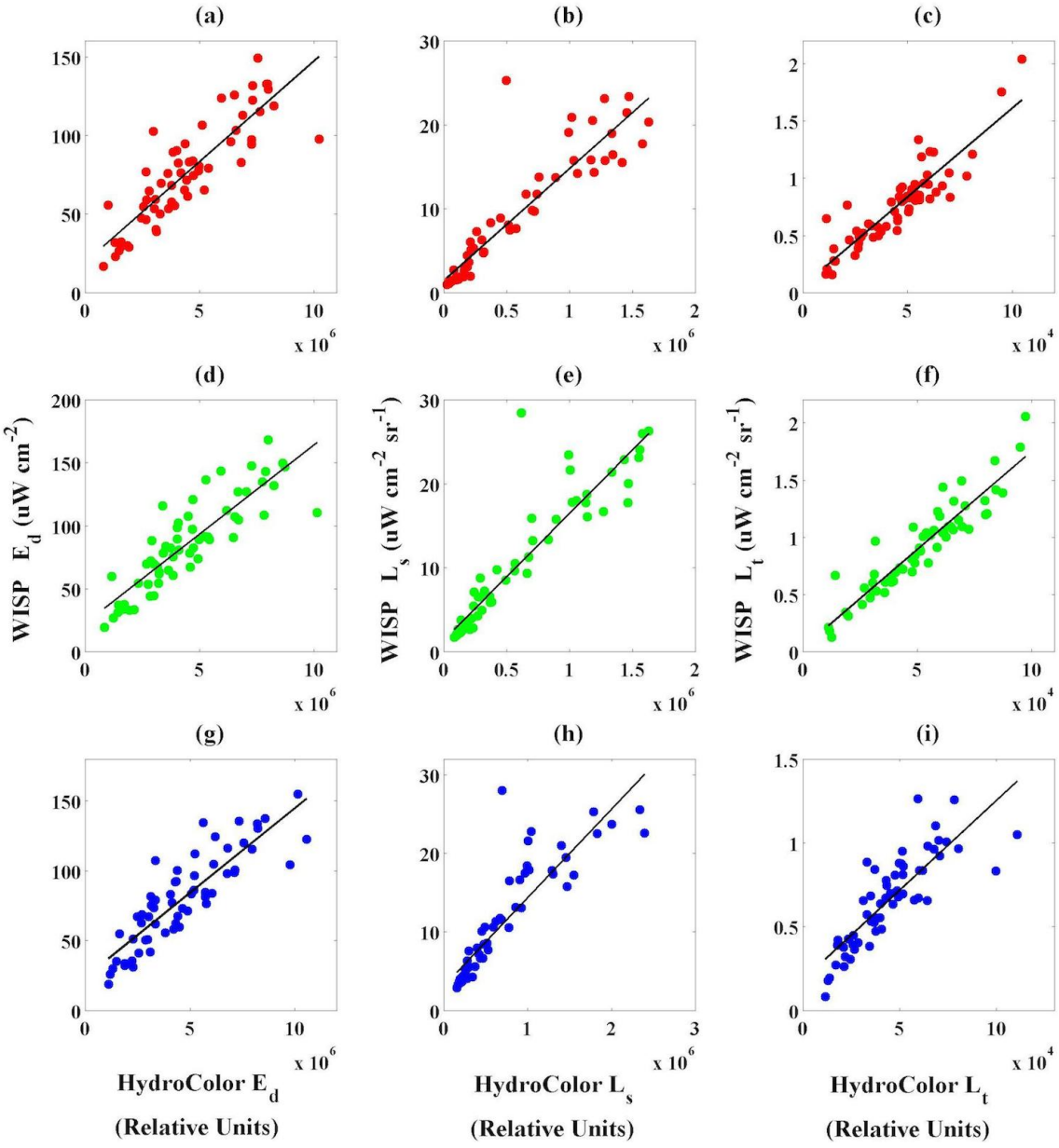

Figure 4.8. Comparison of HydroColor and WISP measurements of E_d, L_s, and L_t. This figure shows data from the red (row 1), green (row 2), and blue (row 3) color channels of the camera.

Table 4.1. Statistics for type-I linear regressions in figure 4.8

Figure	Property	Channel	Slope ($*10^{-5}$)	Intercept	R^2	RMSE
4.3a	E_d	Red	1.28	19.37	0.75	16.26
4.3b	L_s	Red	1.34	1.45	0.83	2.98
4.3c	L_t	Red	1.56	0.06	0.81	0.15
4.3d	E_d	Green	1.42	22.36	0.75	73.07
4.3e	L_s	Green	1.51	1.41	0.86	3.00
4.3f	L_t	Green	1.72	0.03	0.87	0.14
4.3g	E_d	Blue	1.21	23.56	0.75	16.15
4.3h	L_s	Blue	1.13	3.07	0.78	3.36
4.3i	L_t	Blue	1.07	0.18	0.69	0.15

To further investigate how well HydroColor can measure R_{rs}, each component of Eq. 3.9 can be looked at individually. When interpreting this data it is important to remember that it is raw data from the camera prior to taking any ratio of values. Therefore, it may contain biases due to white balance and variations in sensitivity. However, its examination can still provide some useful conclusions.

The data from figure 4.8 helps to confirm our assumption that any error or calibration factor will cancel out in the ratio. The slope values for E_d, L_s, and L_t are similar within each channel (table 4.1). This also indicates that the conversation from the relative radiance of the gray card to the relative downward irradiance is correct. This comparison also show that HydroColor's measurement of E_d is more variable then the other two radiance measurements. This could be a result of placement of the gray card relative to the WISP's irradiance sensor. The gray card was always placed in a low area so a picture could be taken at a downward angle. The WISP irradiance sensor was typically at eye level. In any case, it shows that the HydroColor's measurement of E_d can use the most improvement.

4.3 Turbidity, Particle Concentration, and Backscattering

As discussed in the introduction, the reflectance of the water is directly related to the particulate and dissolved material in the water column. The concentration of suspended particulate matter [SPM] has a large influence on the reflectance of a water body. The magnitude of the backscattering coefficient will have a direct non-linear effect on the reflectance. If backscattering from water and salts are considered to be much smaller than that of particles, the magnitude of the backscattering coefficient is given by the product of the mass specific backscattering coefficient and the concentration of suspended particulate matter:

$$b_{bp} = [SPM] b^*_{bp} \tag{4.1}$$

Where b_{bp} is the particulate backscattering coefficient and b^*_{bp} is the mass specific backscattering coefficient for particles. Mass specific backscattering as a function of wavelength for mineral particles is typically modeled as a power function. Due the occurrence of larger particles, the slope of the mass specific backscatter spectrum tends to flatten out near the coasts (Loisel et al. 2006; Babin[b] et al. 2003). HydroColor measurements are likely to be done in coastal waters where particles tend be larger. Therefore, the shape of backscattering spectrum is assumed to be flat. The exact shape of the backscattering spectrum is not likely to make a significant difference given the uncertainties in the camera measurements.

In the blue and green portions of the spectrum, there is often significant absorptions due to organic material. Both CDOM and chlorophyll absorb strongly in the blue portion of the spectrum. CDOM absorption can also be significant in the green portion of the spectrum. Therefore, the blue and green channels of the camera are not well suited for measuring [SPM]. Chlorophyll does have an absorption peak in the red (at 676nm), however, this peak nearly falls outside the red sensitivity curve of the camera. Therefore, the red channel is best suited for measuring [SPM]. Indeed,

both red and near infrared channels are often used for satellite [SPM] algorithms (Nechad et al. 2010; Sterckx et al. 2007).

In this study I use turbidity measured in nephelometric turbidity units (NTU) as a proxy for [SPM]. The relationship between turbidity and [SPM] is approximately 1 NTU:1 g m^{-3} (Neukermans et al. 2012; Boss et al. 2009). The measurement of turbidity is a much simpler measurement than [SPM] and is the measurement of choice for many environmental monitoring agencies. The turbidity dataset is made up of 58 different measurements spanning multiple platforms (iPod, iPhone 4, iPhone 4), environments (costal ocean, river, estuary), and conditions (sunny, overcast, patchy clouds). The relationship between turbidity and HydroColor measured R_{rs} in the red channel is shown in figure 4.9.

To determine if the relationship between turbidity and R_{rs}(Red) is reasonable, an oceanic radiance model from Gordon et al. (1988) was fit to the data. If we keep the assumption that absorption from from dissolved and particulate organic matter is negligible in the red, the oceanic radiance model is:

$$r_{rs} = 0.0949\left(\frac{b_{bp}}{a_w + a_p + b_{bp}}\right) + 0.0794\left(\frac{b_{bp}}{a_w + a_p + b_{bp}}\right)^2 \tag{4.2}$$

Where r_{rs} is the subsurface remote sensing reflectance, a_w is the absorption of pure water, and a_p is the absorption due to particles. We can turn this into a function we can fit to our data by combining eq. 4.1 and eq 4.2:

$$r_{rs} = 0.0949\left(\frac{[SPM]b^*_{bp}}{a_w + [SPM](a^*_p + b^*_{bp})}\right) + 0.0794\left(\frac{[SPM]b^*_{bp}}{a_w + [SPM](a^*_p + b^*_{bp})}\right)^2 \tag{4.3}$$

Where b^*_{bp} and a^*_p are the fitted variables. The absorption due to water (a_w) was calculated by a weighted average of the pure water absorption spectra from Pope and Fry (1997) using the iPod red sensitivity curve form figure 2.1 as weighting. The absorption due to water seen by the red channel is 0.2479 m^{-1}.

Before fitting the model to the data, the HydroColor measured R_{rs}(Red) was propagated to below the surface. The subsurface remote sensing reflectance r_{rs}(Red) was calculated using an equation from Lee et al. 1999:

$$r_{rs} = \frac{R_{rs}}{0.5 + 1.5R_{rs}} \tag{4.4}$$

The radiance model was fit to the data by minimizing the sum of the absolute difference between the model and the HydroColor measured r_{rs}(Red). The standard deviation (when available) of r_{rs}(Red) were used to weight the fit. One outlier was removed using the same iterative fitting process described in the previous section.

Fitting the radiance model to the turbidity and R_{rs}(Red) data provided a b^*_{bp} value of 0.010 m^{-1} and an a^*_p value of 0.0086 m^{-1}. It is important to remember that these values are the effective b^*_{bp} and a^*_p values for the red channel of the camera, which spans a large portion of the visible spectrum. If we keep our assumption of a flat mass specific backscattering spectrum, the fitted b^*_{bp} simply gives the magnitude of the mass specific backscattering spectrum. A value of 0.01 m^{-1} is well within the range of values seen in the environment (Neukermans et al. 2012). The fitted value for a^*_p is slightly harder to interpret since the mass specific absorption spectrum of particles tends to be an exponential function. However, a simple example of an absorption spectrum that would provide the value of 0.0086 m^{-1} after a weighted average is $a^*_p = 0.015e^{-0.01(\lambda-550)}$ (using the iPod red sensitivity curve). Both the magnitude and slope of this function are well within the value seen in the environment (Babin and Stramski 2004; Estapa 2011). Therefore, the relationship between turbidity (or [SPM]) and HydroColor R_{rs}(Red) agrees well with what is predicted from remote sensing theory. The error between the modeled and measured R_{rs}(Red) values is likely caused by the errors in ρ and variations in b^*_{bp} and a^*_p that are undoubtedly present in such a spatially large dataset.

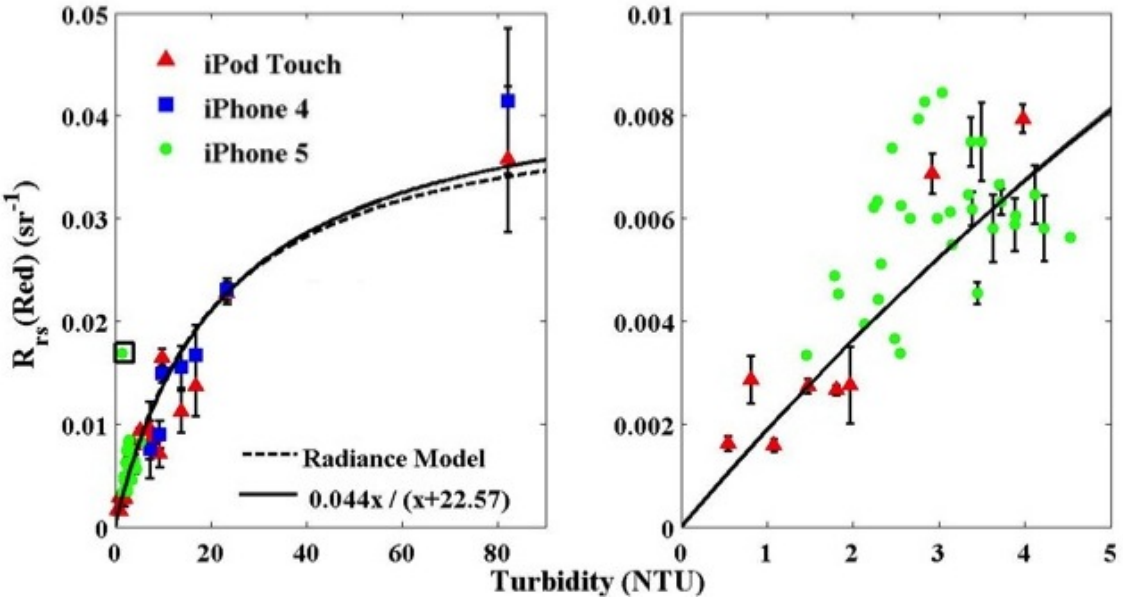

Figure 4.9. Relationship between turbidity and HydroColor R_{rs}(Red). The figure on the right is a closer view of the lower turbidity values plotted in the left figure. Error bars display the stand error (when replicate measurements were available). The one boxed data point identifies an outlier that was not included in the fitting of the radiance model or regression line. The solid lines and dash lines show the fitted relationships described in section 4.3. The radiance model and regression line lie on top of one another in the right plot. For the solid line $R^2 = 0.93$ and RMSE $= 0.003$ sr^{-1}.

For simplicity, a reduced radiance model was also fit to the data. The shape of the R_{rs}(Red)-turbidity relationship can be captured using the following equation:

$$R_{rs}(Red) = \frac{Tur * x_1}{x_2 + Tur} \tag{4.5}$$

Where x_1 and x_2 are the fitted variables. The same method for fitting the full radiance model is used again to fit eq. 4.5 (figure 4.9). The simplified model is used by HydroColor to estimate turbidity from R_{rs}(Red):

$$Tur = \frac{22.57 R_r(Red)}{0.044 - R_{rs}(Red)} \tag{4.6}$$

Using this equation, the median percent error in retrieval of turbidity based on R_{rs} was 24%. The flattening of the turbidity-R_{rs}(Red) relationship at higher turbidity

values can lead to large errors. More data must be collected in higher turbidity environments in order to determine HydroColor's limit of turbidity measurement.

Turbidity in NTU are the official units used by the Environmental Protection Agency (EPA). However, the international standard for the measurement of turbidity is in units of FNU. The differences between the two measures of turbidity are the type of light source used to illuminate the sample. For the measurement in NTU, a Tungsten lamp with a color temperature between 2200-3000° K must be used. To measure in FNU, the light source must be at 860nm with a bandwidth of 30nm (ISO 7027). However, both methods will provide similar values of turbidity for values less than 100 NTU/FNU (Mylvaganam et al. 1998).

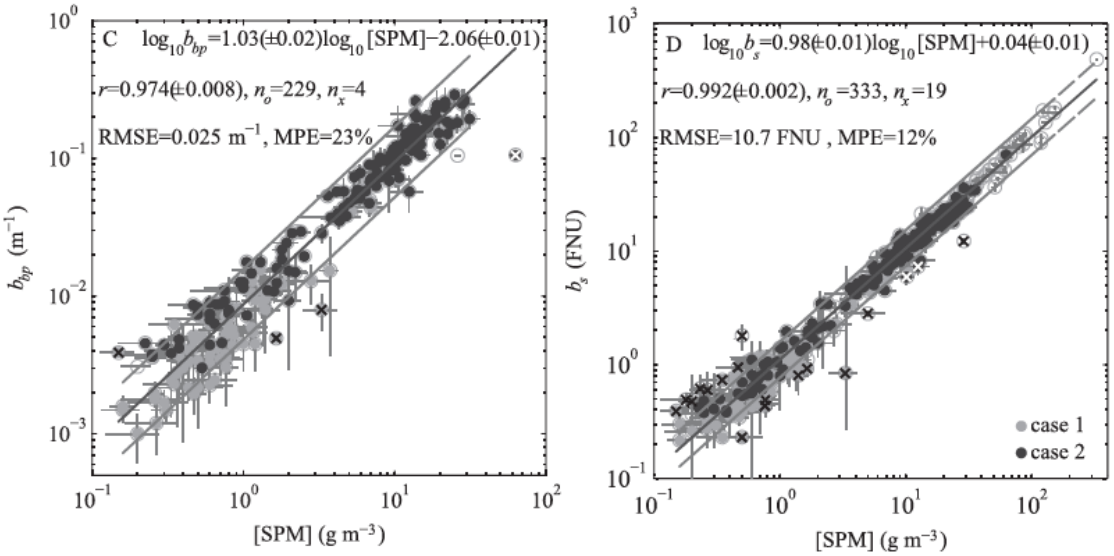

Figure 4.10. Relationship between SPM, turbidity, and backscattering (reproduced from Neukermans et al. 2012). Backscattering in the left plot was measured at 650nm.

Turbidity (or side scattering) is directly related to the both backscattering and the concentration of suspended particulate matter [SPM]. HydroColor uses the relationship from Neukermans et al. (2012) for conversation of turbidity to [SPM] (as opposed to 1 NTU:1 g m^{-3}). This paper compares 333 measurements of both

turbidity (FNU) and [SPM] from both case 1 and case 2 waters (figure 4.10). The relationship between turbidity (FNU) and [SPM] is used by HydroColor to provide users with an estimate of [SPM]:

$$log_{10}[SPM] = 1.02 log_{10}(Tur) - 0.04 \tag{4.7}$$

It is also possible to estimate the particulate backscattering coefficient in the red (b_{bp}) from turbidity or [SPM]. To estimate b_{bp}, HydroColor first propagates R_{rs}(Red) to below the surface using Eq. 4.4. Then HydroColor solves Eq. 4.3 for b_{bp} using a constant a_p^* value of 0.0086 m^{-1} (determined from fitting the full radiance model on page 37), and a_w equal to 0.2479 m^{-1} (from weighted integration of the pure water absorption spectrum from Pope and Fry 1997 by the red sensitivity curve).

4.4 Chlorophyll

Chlorophyll concentration can have a strong effect on the shape of the R_{rs} spectrum. As discussed in the introduction, an increase in chlorophyll concentration causes the reflectance in the green to increase and the reflectance in the blue to decrease. It should be possible to detect this change in reflectance using the blue and green channels of the camera.

However, a simple band ratio for chlorophyll is sensitive to changes in SPM. An increase in SPM will elevate the entire R_{rs} spectrum, which can lead to different ratio values even though chlorophyll has remained constant. Thus, band ratios will not work well in case 2 waters, where SPM can be made up of mineral particles. For HydroColor, an adjusted ratio technique is used where the reflectance in the red is subtracted before the ratio is calculated:

$$C_{chl} = \frac{R_{rs}(Blue) - R_{rs}(Red)}{R_{rs}(Green) - R_{rs}(Red)} \tag{4.8}$$

Subtracting R_{rs}(Red) will partly remove the effect of scattering by particles in order to better quantify the effects of absorption. The value of C_{chl} should decrease with increasing chlorophyll concentration. The decrease should be nonlinear, as predicted by the radiance model from Gordon et al. (1988).

There were only a limited number of chlorophyll measurements collected in parallel with HydroColor. For three HydroColor measurements in the Kara Sea and for 12 HydroColor measurements in the Columbia River, particulate absorption and attenuation spectra were collected using an AC-s. The AC-s was used to measure absorption and attenuation of raw seawater and filtered seawater. The difference between the two spectra provided the absorption and attenuation due to particles. Chlorophyll was derived from the particulate absorption spectra using the absorption line height at 676nm (Roesler and Barnard 2014). For the Columbia River data, the AC-s measurements were all made at a depth of 2-3 meters. For the Kara Sea, AC-s measurements were made at the surface. For 4 measurements along the coast of Maine, extracted chlorophyll data was available (as described in section 4.1.2).

For the data collected in this study, there is a weak relationship between C_{chl} and chlorophyll concentration (figure 4.11). In reality, the relationship between C_{chl} and chlorophyll concentration is likely much better then what is seen in figure 4.11. The majority of the chlorophyll data is subsurface data from the Columbia River. The remote sensing reflectance is obviously most influenced by surface water, especially in coastal areas where chlorophyll and SPM are high. In contrast, the surface values for extracted chlorophyll collected on the Maine coast show a nice relationship to C_{chl}. Extracted chlorophyll was only collected at an inner estuary and outer estuary station, however, it interesting to look at the value of C_{chl} between these stations. A gradient can clearly be seen with distance along the estuary (figure 4.12). Both the iPod touch and iPhone 5 are able to detect the change in chlorophyll that is less

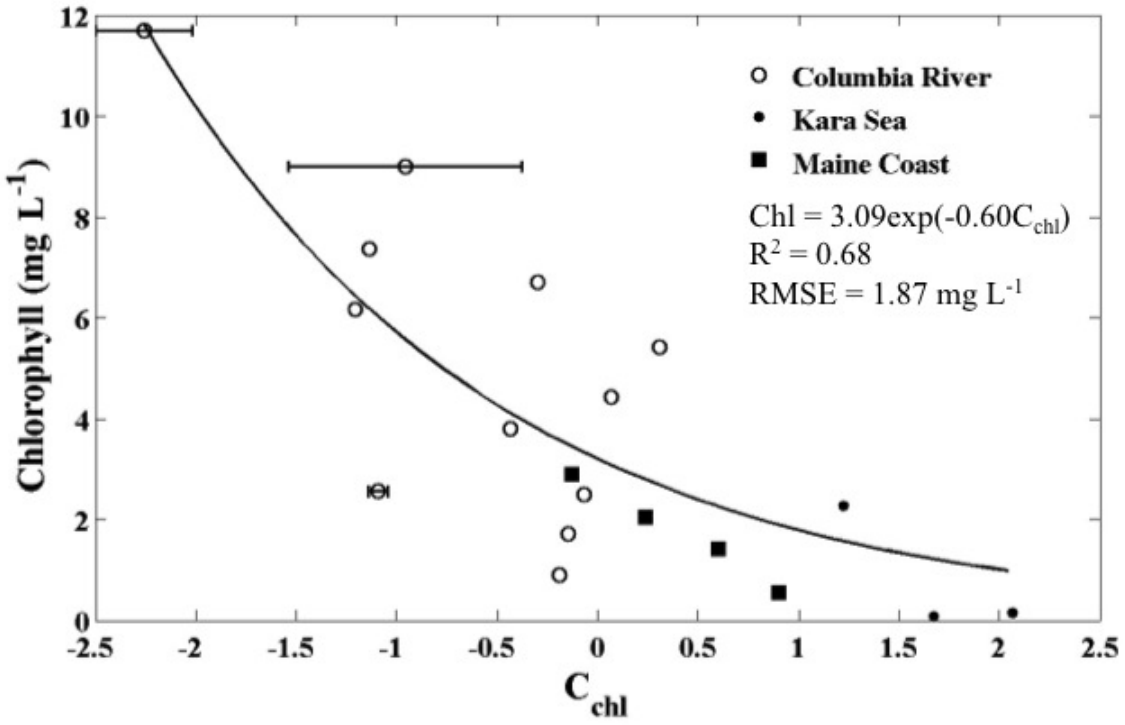

Figure 4.11. Relationship between C_{chl} and chlorophyll concentration. In the Kara Sea and Columbia River, chlorophyll concentration was measured using absorption line height of the particulate absorption spectrum measured by an AC-s. Along the Maine coast chlorophyll concentration was measured via filtration and extraction. It is import to note that the Columbia River data points represent subsurface chlorophyll (2-3m).

than 1 g m^{-3}. Values for C_{chl} are slightly different for each device, possibly owing to the larger bandwidth of the iPhone 5 green filter.

4.5 Photosynthetically Active Radiation

There is potential for HydroColor to also provide an estimate of photosynthetically active radiation (PAR). This is a difficult measurement to make using a camera because it requires the camera to measure radiance absolutely, not relatively. As mentioned before, the sensitivity of the camera to light may be affected by cleanliness of lens, temperature, age, and device manufacturer. With these considerations

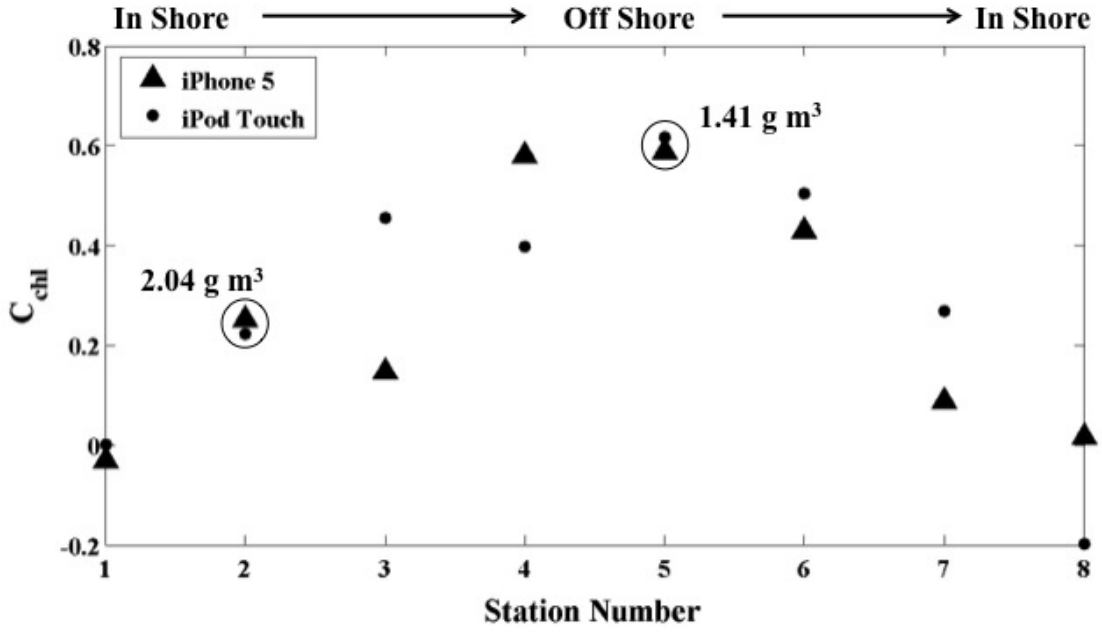

Figure 4.12. C_{chl} along a transect in the Damariscotta River Estuary in Maine. For the two stations where chlorophyll concentration was measured via filtration and extraction (circled), the concentration are provided on the graph.

in mind it may still be possible to obtain a rough estimate of PAR from the gray card image. Since PAR is measured over the whole spectrum, an estimate of PAR can be obtained by summing the RGB values before normalizing by the exposure:

$$B_{rel} = \frac{R + G + B}{\alpha} \tag{4.9}$$

Where B_{rel} is a relative measure of brightness and α is the exposure time. It would be expected that the relative brightness of the gray card would increase as a linear function of PAR. To tests this hypothesis, the E_d spectra from the WISP were integrated from 400 to 700nm to provide a measure of PAR in W m^{-2}. The relative brightness of the gray card was calculated using Eq. 4.9, where the RGB values used in the equation were the average RGB values taken over a 200x200 pixel region at the center of the image.

There exists a weak relationship between relative gray card brightness and PAR (figure 4.13). Some of the scatter in the data is likely due to the fact that the Hydro-

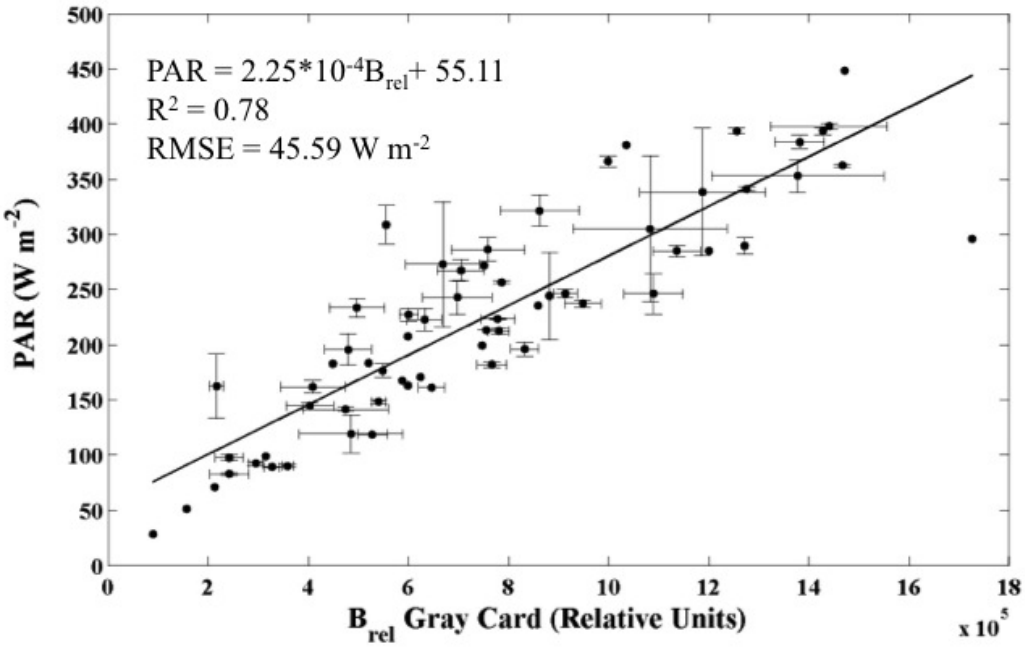

Figure 4.13. Gray card brightness as a function of PAR. Error bars show the standard error when available.

Color and WISP measurements were taken sequentially instead of simultaneously. Therefore, the sky conditions, and PAR, may have changed between when the gray card image was taken and when the WISP measurement was taken. Even with all of these uncertainties it is encouraging to see a relationship emerge. In order for HyrdoColor to provide a PAR product, further tests will have to be preformed in a more controlled environment.

Another potential method for measuring PAR is using the internally calculated APEX brightness value (b_v). The brightness value is defined as (JEITA 2010):

$$B_v = log_2\left(\frac{B}{NK}\right) \tag{4.10}$$

Where B is the average scene luminance (cd cm^{-2}), N is speed scaling constant, and K is the reflected light meter calibration constant. Therefore, the brightness value increases as the $\log_2$ of average scene luminance. The response of B_v to increasing radiance of a diffuse white light is shown in figure 4.14. However, this curve was

generated over a short period of time using a single device (iPod Touch) held in one orientation.

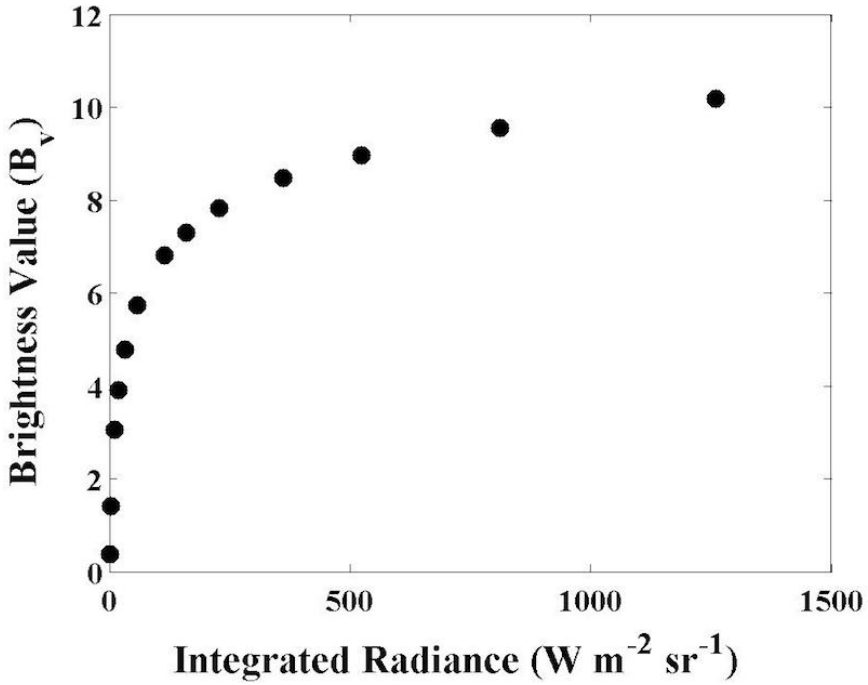

Figure 4.14. Brightness value (B_v) as function of integrated radiance.

Unfortunately, the brightness value was not recorded for any of the HydroColor measurements made in this study. Attempting to determine PAR (or any absolute measure of radiance) was not the initial intent of this study. However, during the Arctic field work, simple camera images were collected in place of HydroColor measurements. The brightness value was stored in EXIF data of these images. The relatively few data points show a tight relationship between 2^{B_v} and PAR (measured by the shipboard PAR sensor) (figure 4.15). The only draw back of using B_v is that it represents the brightness of the entire image. Therefore, the reflectance of the surface the gray card is resting on could have a large impact on B_v. A solution to this is the fill the entire image of the gray card. However, this is not ideal because it requires the camera user to be very close to the gray card. This may shade the

gray card from a significant amount of skylight. It will require further investigation to determine if gray card B_v can be used as a robust estimator of PAR.

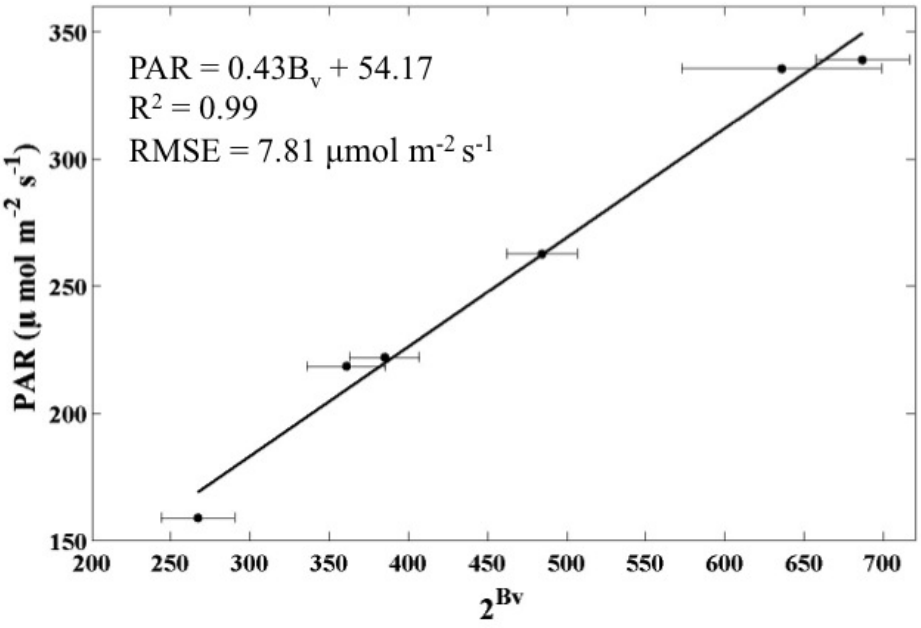

Figure 4.15. PAR as a function of brightness value (B_v). Error bars show the standard error.

CHAPTER 5

DISTRIBUTION

Mobile devices were targeted in this study because once the algorithms were completed they could be widely distributed via this platform. Creation of the HydroColor application required a significant amount of programing to make an intuitive user interface. Once completed the app was made available to people worldwide on the Apple App Store. HydroColor is currently available on the Apple App Store for $2.99.

5.1 User Interface

During the field tests of HydroColor, it could only be used by persons with prior knowledge of HydroColor's operation. Before distribution, a user interface needed to be created that would walk users through the collection of the three images. Apple provides a suit of tools for the development of such an interface. HydroColor was programmed in full using Xcode which is an environment for programing in Objective-C.

5.1.1 About View

Upon first launching HydroColor, a screen displaying information about the app is displayed (figure 5.1). This screen is meant to provide a succinct description of what HydroColor measures, what is needed to use it, where it can be used, and how it should be used. Text displayed on the opening screen in version 1.1 is as follows:

WHAT IT PROVIDES:

HydroColor provides a simple above water method to measure the reflectance of natural water bodies. Using the measured water body reflectance, HydroColor is able to provide an estimate of water turbidity (NTU), suspended particulate matter (SPM) (g/m^3), and the backscattering coefficient in the red. Uncertainties are provided for all parameters computed by HydroColor. In the near future more water quality parameters will be added to HydroColor (e.g. chlorophyll concentration).

HOW TO USE IT:

To use this application you will need a photographers gray card and access to a deep, unshaded patch of water. The gray card is a piece of paper or cardboard with a known 18% reflectance value. They can be purchased at photography shops or online for a few dollars. For best results, use HydroColor in the deepest area accessible (docks, piers, and wharves provide the best locations). If the bottom is visible, this area is too shallow to use HydroColor.

The first image you need to collect with HydroColor is of the photographers gray card. Place the card on a level surface near the measurement area. Be sure the card is in an unshaded area near where you plan to take the water image. An inclinometer and a compass will direct you to the correct angle to take the photograph. When the green indicators match up on each, you are holding the phone in the correct position. Ensure your shadow is not covering the card. The card should fill the white square that appears over the image.

The following two pictures are of the sky and the water surface. The order in which these pictures are taken does not matter. The inclinometer and compass will direct you to the correct angle for these images as well.

Once you are happy with your images, the Analyze Images button will calculate and analyze the reflectance data. The data will be automatically saved to you library. More detailed information about the measurement is written to text file that can be downloaded to a computer from the HydroColor documents folder (accessible in iTunes).

HOW IT WORKS:

HydroColor was developed by Thomas Leeuw and Emmanuel Boss at the University of Maine. More information can be found here: http://misclab.umeoce.maine.edu/research/HydroColor.php

HydroColor v1.1

5.1.2 Data Collection View

The data collection view can be navigated to by pressing the 'Collect Data' button at the bottom of figure 5.1. This view is designed to handle the location information and begin walking users through image collection. Upon entering this view the application attempts to acquire the users latitude and longitude using the iPhone GPS. HydroColor will search for 8 seconds to find a GPS coordinate that is accurate to within less then 200m. New coordinates will be acquired every 5 minutes automatically or when the user selects the 'Update GPS' button. The user also has the option to enter their own latitude and longitude if they are in an area with no GPS signal. If the users coordinates are acquired via GPS or user entered, the users location will be displayed on a map.

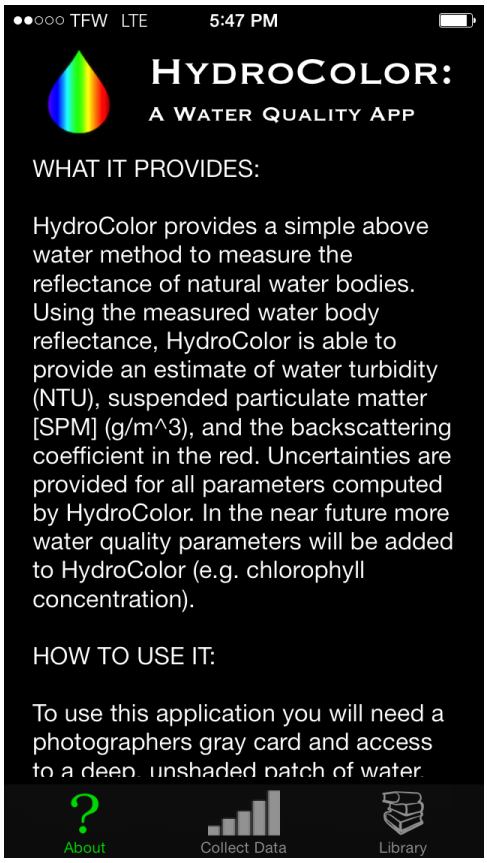

Figure 5.1. Initial screen displayed upon launching HydroColor. This screen displays scrollable text containing basic information about HydroColor. The supporting website and version number is displayed at the bottom of the scrollable text.

Three icons are displayed as placeholders for the three images (figure 5.2 left). The sky and water images are initial grayed out, forcing users to start with the gray card image. This is done in order to lock the white balance on the gray card before continuing to the sky and water images. Selecting the gray card icon will send users to the capture view, described in the next section. After collecting the gray card image, the sky and water icons are no longer grayed out and can be selected in any order. After the images are collected they will be displayed in place of the gray card, sky, or water icons (figure 5.2 right).

After a full set of images is collected, the 'Analyze Images' button is no longer grayed out. Selecting this button will prompt users to enter a name for the mea-

Figure 5.2. HydroColor data collection view. This display is meant to acquire and display GPS information and to begin walking users through image collection. The left and right screenshots show the data collection view before and after image collection.

surement. After entering a name, the images are analyzed, resized, and saved to the HydroColor documents folder. A line of data is also written to the text file 'HydroColor_Datafile' in the HydroColor documents folder. The data written to the file contains: date, time, measurement name, lat, lon, GPS accuracy, sun zenith, sun azimuth, water pitch, water heading, water exposure, sky pitch, sky heading, sky exposure, card pitch, card heading, card exposure, R_{rs}(Red), R_{rs}(Green), R_{rs}(Blue), turbidity, [SPM], and backscatter red (chlorophyll and PAR will be included in a later version). The uncertainties for all HydroColor products are also included in the text file. The text file is meant to provide people with an easy way to download

the data from their phone. It contains sun angles, device angle, and GPS accuracy, which can be used for quality control. Exposure times are provided in case users wanted to retrace the HydroColor calculations themselves. The only thing not provided to the user is the full resolution images. HydroColor resizes the images in order to save space. Theoretically the reduced resolution image still contains the same information and could be used retrace the HydroColor calculations. We can assume that the gray card, sky, and water are relativity uniform in color and brightness, therefore, the resolution of the camera is not important (i.e the same measurement could be made using one big pixel).

5.1.3 Capture View

The most important part of HydroColor is the image capture screen. This screen is used to both direct users to the correct angles and to collect the image. The compass display in the lower left is used to direct users to the correct azimuth angle (figure 5.3). The two green arrows surrounding the compass are rotated according to the output of the sun model. They are rotated such that when the north arrow is aligned with one of the arrows the long axis of the phone is pointed 135° from the sun. There are two arrows because the image can be taken at ±135° from the sun. It has been observed that electromagnetic interference (onboard a ship for example) can cause the compass display to read incorrectly. This can lead to incorrect measurement angles if the user does not recognize that the compass is not pointing North.

To the left of the image is an inclinometer display. The green bar will move up and down as the pitch of the phone changes. For the gray card and water images, the green bar falls between the two green arrows when the optical axis of the camera is 40° from nadir. For the sky image the displays are aligned when the optical axis of the camera is 130° from nadir.

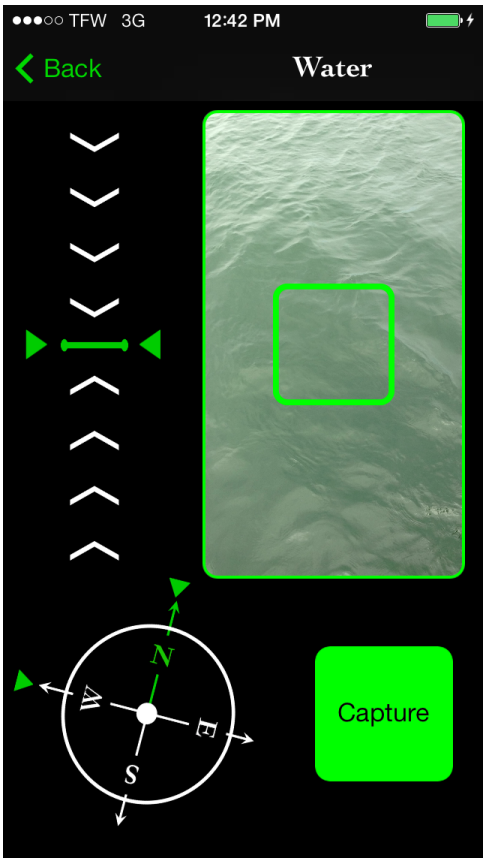

Figure 5.3. HydroColor image capture screen

When both the inclinometer and compass are correctly aligned the capture button and image boarder turn green (as seen in figure 5.3). The capture button and image boarder are white when the compass and inclinometer are not correctly aligned. Upon capturing the image, data about the capture is saved in an array. The zenith and azimuth angles of the device and exposure values are saved for all images. When the water image is taken the date, time, and sun angles are also saved.

5.1.4 Library and Data Viewing

Once a measurement has been collected it is stored in the HydroColor data file. The data in the text file can be directly accessed inside HydroColor. Navigating to

the library page will display a list of past measurements. The user provided name, date, time, and thumbnail of the water image are displayed in the library (figure 5.4). These entries can be selected to open up a page about the measurement. The page displays a graph of the relative reflectance for each channel, a table of values, and a thumbnail of the gray card, sky, and water images. The table in the center of the data viewing screen is scrollable allowing users to view the: date, time, turbidity, [SPM], b_{bp}(Red), R_{rs}(Red), R_{rs}(Green), R_{rs}(blue), latitude, and longitude. The uncertainties for all measured or derived values are also provided.

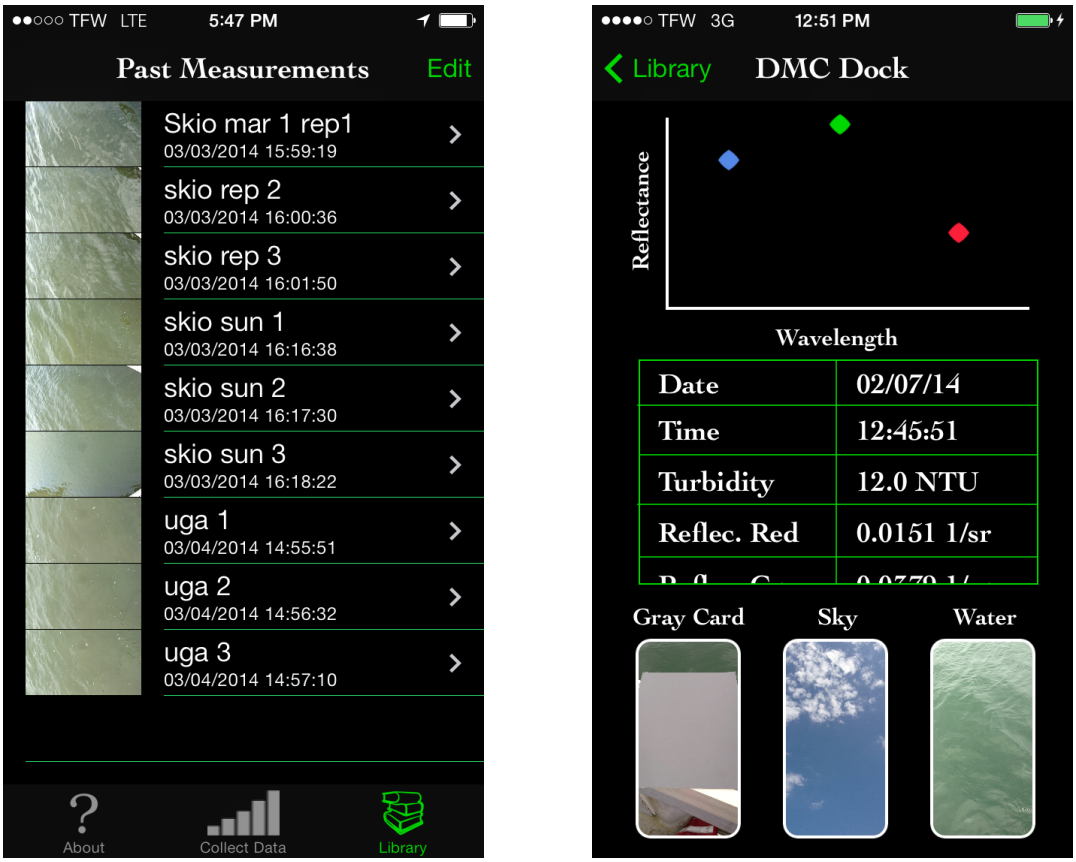

Figure 5.4. Library and data viewing screens

Entries can also be deleted in the library view. Selected the edit button in the upper right will allow the users to delete measurements from the HydroColor data file. When a measurement is deleted, the line of text in the text file corresponding

to the measurement is removed. The image thumbnails are also deleted from the device.

5.2 Downloads

HydroColor was released on the Apple App Store on 2/14/14. The price of HydroColor at the time of publishing was $2.99. Proceeds from HydroColor are reinvested into improving and expanding HydroColor (section 6.1 'Improvements' will give an idea of what this money will be used for). The money will also ensure HydroColor remains on the App store, which costs $100.00 a year.

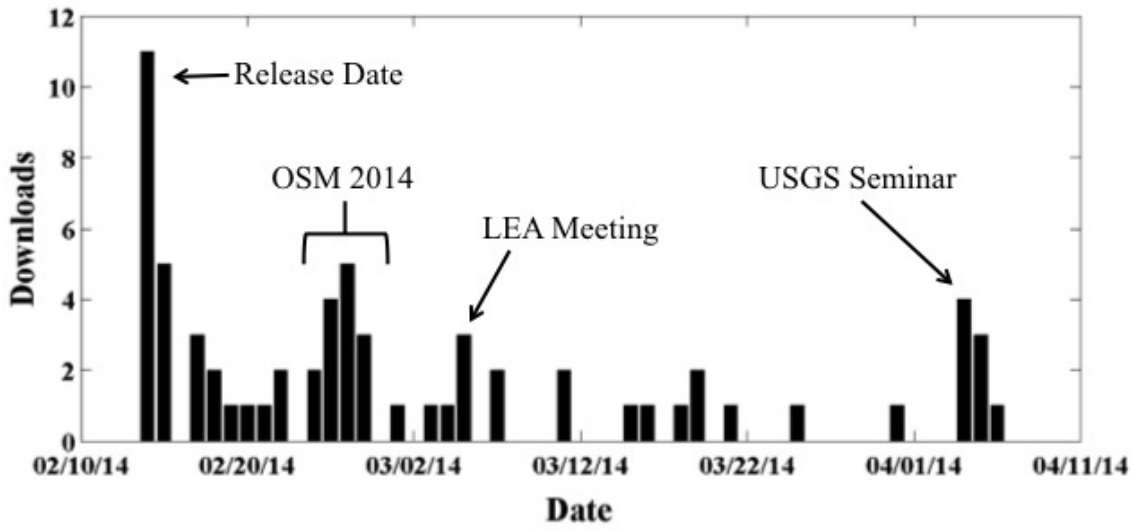

Figure 5.5. HydroColor downloads over time. Notable events include the release date of HydroColor, a poster on HydroColor at the 2014 Ocean Science Meeting (OSM 2014), a presentation to the Lake Environmental Association of Maine (LEA), and a seminar at the USGS office in Sacramento, CA.

As of 04/23/14, 70 copies of HydroColor have been downloaded. Downloads are primarily in the USA, however, there have also been downloads in Canada, Germany, UK, Philippines, and the Netherlands. HydroColor serves a very specific purpose, so it is not likely it will be downloaded by the casual iPhone user. Therefore, it is important to market HydroColor to the right audience. HydroColor was

well received at the 2014 Ocean Sciences Meeting, which is evidenced by elevated downloads (figure 5.5). Downloads peaked on 2/26/14, the day I presented a poster on HydroColor at the Ocean Sciences Meeting. Another peak in downloads corresponds to a presentation I gave to the Lake Environmental Association of Maine on 3/5/14. A significant number of downloads also followed a seminar I gave on HydroColor at the U.S. Geological Survey (USGS) office in Sacramento, CA.

CHAPTER 6

CONCLUSION

6.1 Improvements

This study has provided a significant amount of evidence supporting HydroColor's ability to measure remote sensing reflectance, turbidity, [SPM], b_{bp}, chlorophyll, and potentially PAR. However, there are several improvements that can be made to HydroColor. To implement many of the improvements described in this section it will require significantly more data then is currently available.

The first improvement involves the basic measurement of light with the camera. The measurement of light with the camera can be improved by incorporating ISO speed in addition to exposure time. Exposure time can change orders of magnitude and therefore plays a much larger roll than ISO speed. However, the ISO speed can vary between images. The ISO speeds of the images collected in this study were not recoverable from images, therefore, it is not possible to apply ISO corrections to this data set. The second improvement is a gamma correction to the RGB values. A gamma correction ensures the linearity of the RGB values as a function of radiance. In this study, applying a traditional gamma correction with an exponent of 2.2 made no improvement in the measurement of R_{rs} or retrieval of the water quality parameters. Creation of a unique gamma correction function for HydroColor may improve results. In any case, it is clear that the current method works regardless of gamma or ISO correction. However, further investigation into these parameters may allow for a tighter turbidity or chlorophyll calibration.

Another improvement is to make the skylight reflection factor ρ a dynamic variable. As described in section 3.4, ρ is dependent on wind speed. Assuming a data

connection is available, the wind speed at the current location can be looked up on the web. A look up table of ρ values as a function sun zenith and wind speed can be hard coded into the HydroColor software. Therefore, ρ can vary with the users current conditions. Of course this method is only accurate if the user is near a facility that measures the wind speed. It also depends on how well the sea states can be modeled from winds speed in coastal environments. Another method of determining sea state would be to use a series of water images as oppose to a single image. For example 5 images could be taken one second apart. If the water was calm, the five images would be very similar to each other. If the water was choppy, there would be lots of variability between the images. The variability in the images could be used to assign a value for ρ or be used to better quantify the measurement uncertainty. The same technique could be applied using a short video of the water's surface.

The value of ρ is also depended on cloud cover. Currently HydroColor has no way of assessing cloud cover. It would be difficult to determine cloud cover based on weather data because cloud conditions can be very localized. It may be possible to determine cloud cover by an automated analysis of the sky image. Both the spectral characteristics of the sky image and the patchiness of the image could be used to estimate the amount of cloud cover. A uniform image with high values in the blue channel would indicate clear skies. A uniform image with relatively equal values across all channels would indicate an overcast sky. A patchy image with both blue and white peaks would indicate patchy clouds. Cloud cover could also be determined via user entered values before the measurement is taken. The value of ρ could be adjusted accordingly using a lookup table.

Eventually HydroColor will be available for Android devices in addition to Apple devices. Conversion of HydroColor to Android will make the software available to a much larger audience. This will require characterizing the camera onboard other brands of smartphones (e.g. Samsung, Motorola, LG). The sensitivity curves should

not vary greatly between devices as camera technology is rather standardized on mobile devices (CMOS with Bayer filter). If the sensitivity curves appear similar, it will not require extensive field testing.

The most important improvement to HydroColor is linking the application to an online database. The end goal of the application is to have both scientists and non-scientists submit their HydroColor measurements to an online repository. This will complete the crowdsourcing aspect of this study. However, the database must have a user friendly interface. For crowdsourcing of data to work, the data must be accessible to everyone. This means excellent online tools for data visualization. There is little incentive for average people to make these types of measurements. Citizen scientist will not be excited to submit data to the HydroColor database if the data is inaccessible. If people can go online and view measurements they have submitted, this will encourage further data collection. This type of database may require a significant amount of work, however, it is necessary for a crowdsourcing venture to succeed.

6.2 Broader Impacts

HydroColor has the potential to make a large impact on both the scientific and educational community. There are over a billion smartphone users worldwide. This means there are a billion people carrying a potential water quality instrument. Even if a fraction of a percent of these people were to collect measurements using HydroColor, a respectable global database of water quality measurements could be generated. It has the additional advantage that the measurement tool and method is standardized across the globe. Apple devices are found all across the globe and they all carry the hardware described in this study. Assuming people use HydroColor correctly, the measurement methodology will also be the same across the globe.

Crowdsourcing can also be used to improve HydroColor's calibration. There are numerous organizations and societies that already collect chlorophyll and turbidity measurements using commercial instruments. Users could have the option to submit this data along side their HydroColor measurements. This would improve the calibration by providing data from diverse environments.

HydroColor also has potential to be used as an educational tool. Many students (high school and college) already own smartphones. Therefore, HydroColor is a very small investment while providing an excellent learning tool. The combination of HydroColor and gray card would cost around $8.00 (however, there are app discounts for educational institutions). HydroColor could be used to teach lessons in: environmental monitoring, oceanography, optics, remote sensing, image analysis, and many more. HydroColor can also be used as a public outreach tool. A camera is a tool most people are very comfortable with. HydroColor can show people how a tool as simple as their camera can help them learn about their environment. It can also act as gateway for people to understand less tangible science concepts. For example, HydroColor can provide people with an understanding of what an ocean color satellites measures and why they are a valuable use of our resources.

REFERENCES

Aiken, J., Moore, G.F., Trees, C.C., Hooker, S.B., Clark, D.K. 1995. The SeaWiFS CZCS-type pigment algorithm, *NASA Tech. Memo. 104566(29)*.

Babin[a], M., Stramski, D., Ferrari, G., Claustre, H., Bricaud, A., Obolensky, G., Hoepffner, N. 2003. Variations in the light absorption coefficients of phytoplankton, nonalgal particles, and dissolved organic matter in costal waters around Europe. *Journal of Geophysical Research*, 108(C7): 3211-3231.

Babin[b], M., Morel, A., Fournier-Sicre, V., Fell, F., Stramski, D. 2003. Light scattering properties of marine particles in coastal and open ocean waters as related to the particle mass concentration. *Limnology and Oceanography*, 48(2): 843-859.

Babin, M., Stramski, D. 2004. Variations in the mass-specific absorption coefficient of mineral particles suspended in water. *Limnology and Oceanography*, 49(3): 756-767.

Boss, E. Taylor, L., Gilbert, S., Gundersen, K., Hawley, N., Janzen, C., Johengen, T., Purcell, H., Robertson, C., Schar, D.W.H., Smith, G.J., Tamburri, M.N. 2009. Comparison of inherent optical properties as a surrogate for particulate matter concentration in coastal waters. *Limnology and Oceanography: Methods*, 7: 803:810.

Boyer, J.N. Kelble, C.R., Ortner, P.B., Rudnick, D.T. 2009. Phytoplankton bloom status: chlorophyll a biomass as an indicator of water quality condition in the southern estuaries of Florida, USA. *Ecological Indicators*, 9s: s56-s67.

Bricaud, A., Morel, A., Prieur, L. 1981. Absorption by dissolved organic matter of the sea (yellow substance) in the UV and visible domains. *Limnology and Oceanography*, 26(1): 43-53.

Briones, V., Aguilera, J.M. 2005. Image analysis of changes in surface color of chocolate. *Food Research International*, 38: 87-94.

Carder, K.L., Steward, R.G. 1985. A remote sensing reflectance model of a red-tide dinoflagellate off west Florida. *Limnology and Oceanography*, 30(2): 286-298.

Clarke, G.L., Ewing, G.C., Lorenzen, C.J. 1970. Spectra of backscattered light from the sea obtained from aircraft as a measure of chlorophyll concentration. *Science*, 167(3921): 1119-1121.

Eggleton, J., Thomas, K.V. 2004 A review of factors affecting the release and bioavailability of contaminates during sediment disturbance events. *Environment International*, 30: 973-980.

Estapa, M. 2011. Photochemical reactions of particulate organic matter. Doctoral dissertation, University of Maine.

Goddijn, L.M, White, M. 2006. Using a digital camera for water quality measurements in Galway Bay. *Estuarine, Costal, and Shelf Science*, 66: 429-436.

Goddijn-Murphy, L., Dailloux, D., White, M., Bowers, D. 2009. Fundamentals of in situ digital camera methodology for water quality monitoring of coast and ocean. *Sensors*, 9: 5825-5843.

Gordon, H.R., Brown, O.B., Evans, R.H., Brown, J.W., Smith, R.C., Baker, K.S., Clark, D.K. 1988. A semianalytic radiance model of ocean color. *Journal of Geophysical Research*, 93(D9): 10,909-10,924.

Gordon, H.R., Wang, M. 1994. Retrieval of water-leaving radiance and aerosol optical thickness over the oceans with SeaWiFS: a preliminary algorithm. *Applied Optics*, 33(3): 443:452.

Hinrichsen, D. 1999. The coastal population explosion, in: *Trends and future challenges for the U.S national ocean costal policy*. NOAA.

Hommersom, A., Kratzer, S., Laanen, M., Ansko, I., Ligi, M., Bresciani, M., Giardino, C., Beltran-Abaunza, J.M., Moore, G., Wernand, M., Peters, S. 2012. Intercomparison in the field between the new WISP-3 and other radiometers (TrioOS Ramses, ASD FieldSpec, and TACCS). *Journal of Applied Remote Sensing*, 6: 063615(1-21).

ISO 7027. 1999. *Water quality - determination of turbidity*. International Organizations for Standardization.

JEITA. 2010. *Exchangeable image file format for digital still cameras: Exif Version 2.3*. JEITA CP-3451C.

Knap, A., A. Michaels, A. Close, H. Ducklow and A. Dickson (eds.). 1996. Protocols for the Joint Global Ocean Flux Study (JGOFS) Core Measurements. JGOFS Report Nr. 19, vi+170 pp. Reprint of the IOC Manuals and Guides No. 29, UNESCO 1994.

Kwiatkowski, R.E., Roff, J.C. 1976. Effects of acidity on the phytoplankton and primary productivity of selected northern Ontario lakes. *Canadian Journal of Botany*, 54: 2546-2561.

Lee, Z., Carder, K.L., Mobley, C.d., Steward, R.G., Patch, J.S. 1999. Hyperspectral remote sensing for shallow waters: 2. Deriving bottom depths and water properties by optimization. *Applied Optics*, 38(18): 3831-3843.

Lee, Z., Casey, B., Arnone, R., Weidemann, A., Parsons, R., Montes, M.J., Gao, B., Goode, W., Davis, C.O., Dye. J. 2007. Water and bottom properties of a coastal environment derived from Hyperion data measured from the EO-1 spacecraft platform. *Journal of Applied Remote Sensing*, 1: 011502.

Lee, Z., Pahlevan, N., Ahn, Y., Gerb, S. O'Donnell, D. 2013. Robust approach to directly measuring water-leaving radiance in the field. *Applied Optics*, 52(8): 1693:1701.

Loisel, H., Nicolas, J.M., Sciandra, A., Stramski, D., Poteau, A. 2006. Spectral dependency of optical backscattering by marine particles from satellite remote sensing of the global ocean. *Journal of Geophysical Research*, 111: C09024.

Mobley, C.D. 1999. Estimation of the remote-sensing reflectance from above-surface measurements. *Applied Optics*, 38(36): 7442-7455.

Mylvaganaru, S., Jakobsen, T. 1998. Turbidity sensor for underwater applications. *OCEANS '98 Conference Proceedings*, 1: 158-161.

Nechad, B., Ruddick, K.G., Park, Y. 2010. Calibration and validation of a generic multi sensor algorithm for mapping of total suspended matter in turbid waters. *Remote Sensing of Environment*, 114: 854-866.

Neukermans, G., Loisel, H., Meriaux, X., Astoreca, R., McKee, D. 2012. In situ variability of mass-specific beam attenuation and the backscattering of marine particles with respect to particle size, density, and composition. *Limnology and Oceanography*, 57(1): 124:144.

O'Reilly, J.E., Maritorena, S., Mitchell, B.G., Siegel, D.A., Carder, K.L., Garver, S.A., Kahru, M., McClain, C. 1998. Ocean color chlorophyll algorithms for SeaWiFS. *Journal of Geophysical Reseach*, 103(C11): 24,937-24,953.

Pope, R.M., Fry, E.S. 1997. Absorption spectrum (380-700 nm) of pure water. II. Integrating cavity measurements. *Applied Optics*, 36(33): 8710-8723.

Reda, I., Andreas, A. 2008. Solar position algorithm for solar radiation application. National Renewable Energy Laboratory (NREL). Technical report NREL/TP-560-34302.

Roesler, C.S., Barnard, A.H. 2014. Optical proxy for phytoplankton biomass in the absence of photophysiology: Rethinking the absorption line height. *Methods in Oceanography*, In-press.

Soffer, R.J., Harron, J.W., Miller, J.R. 1995. Characterization of Kodak grey cards as reflectance reference panels in support of BOREAS field activities. Proceedings: 17th Canadian Symposium on Remote Sensing, pp. 357-362, Saskatoon, Sask.

Sterckx, S., Knaeps, E., Bollen, M., Trouw., K., Houthuys, R. 2007. Retrieval of suspended sediment from advanced hyper spectral sensor data in the Scheldt Estuary at different stages in the tidal cycle. *Marine Geodesy*, 30: 97-108.

Tolk, B.L., Han, L., Rundquist, D.C. 2000. The impact of bottom brightness on spectral reflectance of suspended sediments. *International Journal of Remote Sensing*, 21(11): 2259-2268.

Voice, T.C., Weber, W.J. 1983. Sorption of hydrophobic compounds by sediments, soils and suspended solids-I. *Water Research*, 17(10): 1433-1441.

BIOGRAPHY OF THE AUTHOR

Thomas Leeuw was born in Burlington, VT and graduated form Mount Abraham Union High School in Bristol, VT in 2008. He received a B.S. in Marine Science (summa cum laude) from the University of Maine in 2012. During his time at the University of Maine, Thomas has authored and co-authored papers in the peer reviewed journals: *Applied Optics*, *Sensors*, and *Methods in Oceanography*.

Thomas Leeuw is a candidate for the Master of Science degree in Oceanography from The University of Maine in May 2014.